Bulletin of the Seismological Society of America, Vol. 101, No. 3, pp. 1162–1181, June 2011, doi: 10.1785/0120090261

LiDAR-Assisted Identification of an Active Fault near Truckee, California

by L. E. Hunter, J. F. Howle, R. S. Rose, and G. W. Bawden

Abstract We use high-resolution (1.5–2.4 points/m^2) bare-earth airborne Light Detection and Ranging (LiDAR) imagery to identify, map, constrain, and visualize fault-related geomorphology in densely vegetated terrain surrounding Martis Creek Dam near Truckee, California. Bare-earth LiDAR imagery reveals a previously unrecognized and apparently youthful right-lateral strike-slip fault that exhibits laterally continuous tectonic geomorphic features over a 35-km-long zone. If these interpretations are correct, the fault, herein named the Polaris fault, may represent a significant seismic hazard to the greater Truckee–Lake Tahoe and Reno–Carson City regions. Three-dimensional modeling of an offset late Quaternary terrace riser indicates a minimum tectonic slip rate of 0.4 ± 0.1 mm/yr. Mapped fault patterns are fairly typical of regional patterns elsewhere in the northern Walker Lane and are in strong coherence with moderate magnitude historical seismicity of the immediate area, as well as the current regional stress regime. Based on a range of surface-rupture lengths and depths to the base of the seismogenic zone, we estimate a maximum earthquake magnitude (M) for the Polaris fault to be between 6.4 and 6.9.

Introduction

The U.S. Army Corps of Engineers (USACE) owns and operates an inventory of more than 600 dams across the United States (Halpin and Ferguson, 2007) and recently implemented the Dam Safety Assurance Program (DSAP) to evaluate risks to the public posed by these dams as a consequence of potential failure. The Martis Creek Dam, located ~6 km east of Truckee, California (Fig. 1a) and ~56 km upstream from Reno, Nevada, is one of ten dams nationwide that received a Dam Safety Action Class I ranking, indicating urgent and compelling safety concerns.

Completed in 1972, the Martis Creek Dam is a zoned earthen embankment with an impervious blanket on the upstream side. Glacial outwash underlies most of the dam's foundation and left abutment, while layered volcanic rock underlies the right abutment (U.S. Army Corps of Engineers, 1966, 1972; Latham, 1985; and Sylvester *et al.*, 2007). A history of excessive seepage during reservoir test fillings, including sand boils along the downstream toe and seepage along stratigraphic contacts adjacent to the spillway, have prevented the USACE from allowing the dam to fulfill its full design function of flood control and limited water storage. These leakage problems are compounded by a significant seismic hazard (I. Wong *et al.*, unpublished report, 2008, see Data and Resources), based on the presence of two fault zones within 10 km of the dam that may be capable of generating horizontal ground motion near 1.0g, thereby exceeding the seismic-design criteria of 0.1g.

As part of the DSAP evaluation, we acquired airborne LiDAR (Light Detection and Ranging) to provide a detailed digital elevation model to support geotechnical investigations, evaluate surface morphology, and provide data for potential inundation modeling. These data were augmented with aerial photographic imagery and demonstrate the presence of numerous geomorphic features suggestive of Late Pleistocene or Holocene fault surface rupture in the vicinity of Martis Creek Dam.

The LiDAR data presented in this paper were collected in two independent surveys. Merrick and Company flew approximately 260 km^2 in 2006 for the Truckee Donner Public Utility District (TDPUD); the LiDAR data they collected were to be used for infrastructure planning. The second dataset was collected in 2008 by Towell Surveying Mapping and GIS Services and extends from the southern portion of the Sierra Valley to the north shore of Lake Tahoe. The second dataset was collected specifically for tracing the Polaris fault to the northwest and southeast. Both Merrick and Towell generated bare-earth point-cloud datasets (classified ground data) using TerraScan software (see Data and Resources section). For the Merrick data, spot spacing of the laser first returns is approximately 4.3 ± 0.3 points/m^2, and the classified ground data are 2.4 ± 0.3 points/m^2, based on the average density of points from nine randomly selected 2.59-km^2 tiles. The Towell first-return data have a spot spacing of 3.4 ± 0.9 points/m^2, and the classified

ground data are 1.5 ± 0.4 points/m^2, based on the average density of points from eight randomly selected 0.84-km^2 tiles. The classified point-cloud data were imaged using Quick Terrain (QT) Modeler (see Data and Resources section) and modeled as a gridded surface. QT Modeler develops the surface by performing a Delaunay triangulation that mathematically creates a triangulated irregular network (TIN) from the original points. The software then creates the grid according to a user-defined grid spacing (here typically on the order of 1–2 m; however, for large scale maps, we used a spacing of up to 5 m). Elevations from the TIN are then assigned to the vertices of the grid and are retriangulated to create a smoothed topographic surface. No additional processing was applied to the data.

Analysis of these data, using pseudosun angles, vertical exaggeration of 2–2.5 times, oblique perspectives, and extracted profiles revealed a series of linear features across the landscape that extends from southeast of the Martis Valley for at least 35 km northwest past Kyburz Flat (Fig. 1). Along this trace are conspicuous geomorphic and hydrologic features such as scarps in unconsolidated alluvium, elongate depressions aligned with adjacent linear mounds, anomalously deep hillside troughs with little or no contributing drainage area, closed depressions, linear swales, mole tracks, offsets of fluvial terrace risers, right-lateral deflections of creeks and river courses, and shutter ridges, as well as springs and linear seeps. We interpret these features as evidence for a previously unrecognized right-lateral strike-slip fault associated with the northern Walker Lane fault zone and herein refer to this likely active fault as the Polaris fault. Polaris is the name of a 19th-century townsite that was located along the Truckee River, where we have identified progressive tectonic displacement of late Pleistocene terrace risers and other tectonic geomorphic features. The goal of

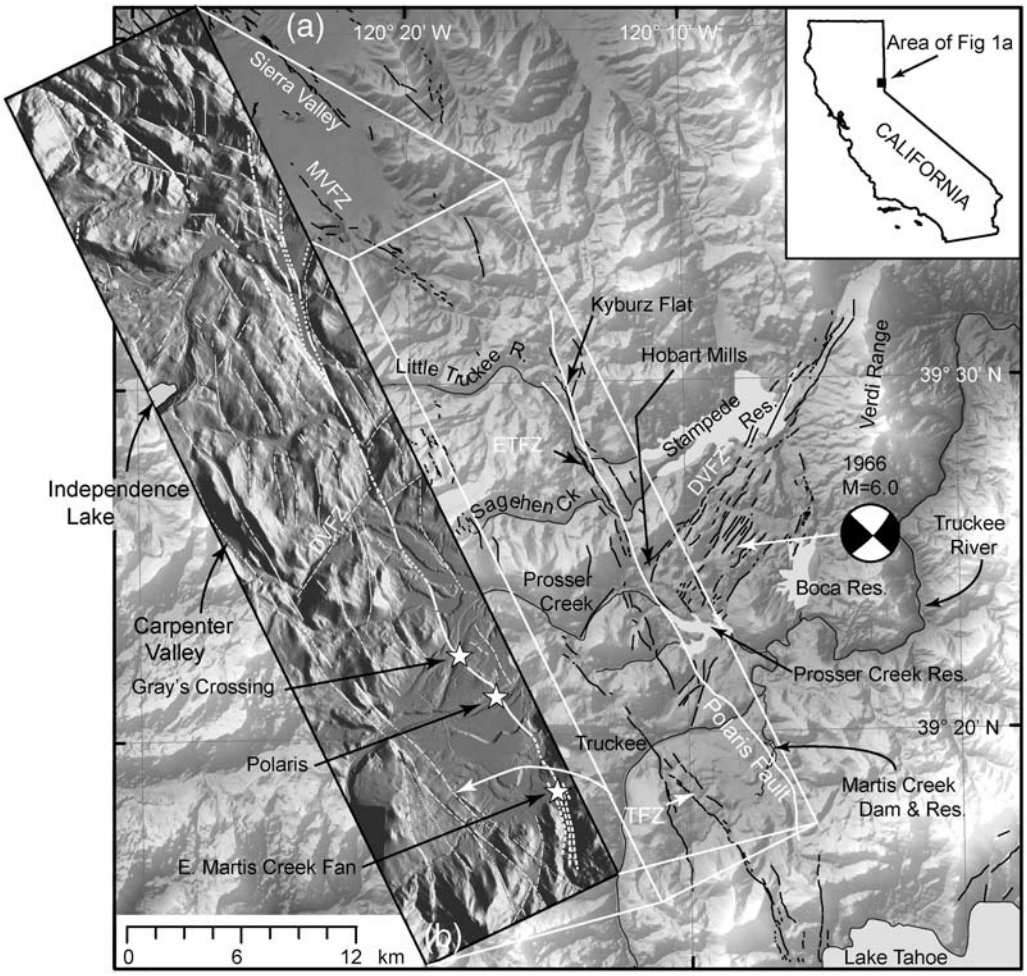

Figure 1. (a) Regional map showing location of the Polaris fault and selected regional faults from the U.S. Geological Survey (USGS) Quaternary Fault and Fold Database (see Data and Resources) and from I. Wong *et al.* (unpublished report, 2008, see Data and Resources: MVFZ, Mohawk Valley fault zone (#25b, from USGS); TFZ, Truckee fault zone (A005, from Wong *et al.*); ETFZ, Eastern Truckee fault zone (A005b, from Wong *et al.*); and DVFZ, Dog Valley fault zone (#27, from USGS). Also shown are the focal plane mechanism and epicenter location of the 1966 Truckee *M* 6.0 earthquake. (b) Inset topographic map showing high-resolution airborne LiDAR imagery, the Polaris fault (bold white line) and subordinate structures (broken white lines) mapped using bare-earth LiDAR. Stars indicate the locations of the East Martis Creek fan, Polaris, and Gray's Crossing sites; also shown are the Martis Creek Dam, and selected geographic features. Illumination is from the east–northeast.

this paper is to characterize the Polaris fault and the previously unrecognized regional extent, provide a preliminary estimate of the minimum tectonic slip rate, discuss the local fault patterns with respect to the regional tectonic setting, and discuss the length of the Polaris fault and seismic hazard implications.

Regional Tectonic Setting

Geodetically measured right-lateral motion between the Pacific and North American plates is primarily accommodated on the San Andreas fault system, with ~20%–25% of the deformation occurring east of the Sierra Nevada microplate (SNP) in the western Basin and Range Province (Dixon *et al.*, 1995; Thatcher *et al.*, 1999; Bennett *et al.*, 2003; Hammond and Thatcher, 2004, 2007). Space geodesy reveals that the SNP is translating northwestward (N40°–45°W) at ~14 mm/yr (Dixon *et al.*, 2000), relative to the stable North American plate (Fig. 2a). The SNP slip vector is oblique (~45°W) to the roughly north-striking normal faults along the eastern escarpment of the SNP and subparallel to the dextral faults of the Walker Lane (Stewart, 1988; Faulds *et al.*, 2005; Wesnousky, 2005b), creating a zone of dextral shear or dextral transtension (Unruh *et al.*, 2003; Schweickert *et al.*, 2004; Wesnousky, 2005a). Thus, the northwest-striking dextral faults of the Walker Lane are favorably oriented to accommodate the large-scale Pacific–North American plate motion east of the SNP. The broader Walker Lane–eastern California shear zone (ECSZ in Figure 2a) is thought to represent an incipient transform plate boundary (Faulds *et al.*, 2005; Wesnousky, 2005a; Faulds and Henry, 2008), and the complexity of faulting within this region is largely attributed to the immature stage of this evolution (Schweickert *et al.*, 2004; Wesnousky, 2005b).

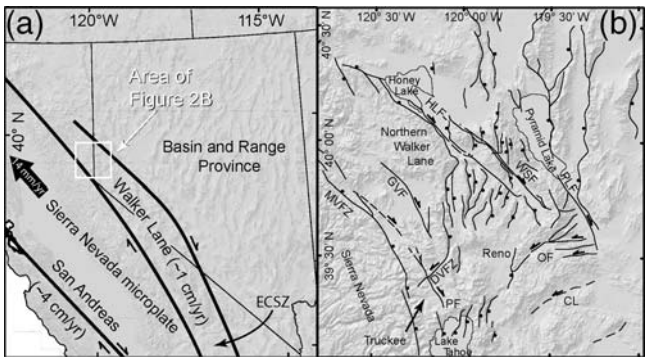

Figure 2. (a) Generalized location map showing the Walker Lane–eastern California shear zone (ECSZ) in relation to the Basin and Range Province, the Sierra Nevada microplate, and the San Andreas fault system, as well as relative motions and rates. (b) Generalized fault map of the northern Walker Lane: PF, Polaris fault; DVFZ, Dog Valley fault zone; MVFZ, Mohawk Valley fault zone; GVF, Grizzly Valley fault; HLF, Honey Lake fault; WSF, Warm Springs Valley fault; PLF, Pyramid Lake fault; OF, Olinghouse fault; and CL, Carson lineament. Barbed arrows show relative motion of strike-slip faults, and black dots shows down-thrown side of normal faults. Parts (a) and (b) are modified from Faulds and Henry (2008).

The Truckee basin lies on the boundary between the SNP and the northern Walker Lane (NWL), also known as the Sierra Nevada—Great Basin boundary zone (SNGBBZ in van Wormer and Ryall, 1980; Zoback, 1989; Schweickert *et al.*, 2004). At the latitude of the Truckee basin, the NWL is a ~100-km-wide zone of spatially overlapping and kinematically linked northwest-trending right-lateral strike-slip faults, northeast-trending left-lateral strike-slip faults, and north-striking normal faults (Bennett *et al.*, 2003; Schweickert *et al.*, 2004; Faulds *et al.*, 2005; Wesnousky, 2005a). It is in this complex zone that ~20% of the dextral shear between the Pacific and North American plates is accommodated with a pronounced increase occurring west of 119° in the NWL (Thatcher *et al.*, 1999; Bennett *et al.*, 2003; Hammond and Thatcher, 2004, 2007). Between the SNP and ~119° W, this increased rate equates to ~6 ± 2 mm/yr of dextral shear in the general vicinity of the Truckee basin and Polaris fault (Thatcher *et al.*, 1999; Dixon *et al.*, 2000; Hammond and Thatcher, 2004, 2007).

In the NWL and the region surrounding the Lake Tahoe and Truckee basin, the dextral transtension appears to be accommodated by spatially and temporally alternating modes of faulting (Wright, 1976; Stewart, 1988; Zoback 1989; Ichinose *et al.*, 1998; Schweickert *et al.*, 2004). In the current-mode conjugate zones of high-angle strike-slip faults (northeast-trending left-lateral and northwest-trending right-lateral) accommodate north–south shortening and east–west extension. In the alternate mode, extension generally perpendicular to the range fronts is accommodated by the normal faults (Ichinose *et al.*, 2003). In the current stress regime (for zones of conjugate strike-slip faulting like the Truckee basin), the maximum principal stress vector (S_1, or P-axis) is oriented horizontally (S_H) in a north–south vertical plane, the intermediate stress vector (S_2) is vertical (S_V) in the same north–south plane, and the minimum principal stress (S_3, or T-axis) is oriented east–west perpendicular to the latter plane ($S_H > S_V > S_3$). In the normal faulting mode, the relative magnitudes of S_1 and S_2 switch within the north–south vertical plane (S_1 vertical), while the T-axis remains oriented east–west ($S_V > S_H > S_3$). According to Zoback (1989), the magnitudes of S_1 and S_2 are similar (i.e., $S_H \approx S_V$), which is consistent with temporally and spatially alternating modes of strike-slip and normal faulting that collectively accommodate the regional transtension over geologic time scales.

Glacial and Alluvial Stratigraphy

The fault-bounded Truckee basin, including the Martis Valley and main stem of the Truckee River east of the town of Truckee, is filled with a succession of Pleistocene ground moraines in the western half and coeval glacial outwash terraces in the eastern half (Birkeland, 1963, 1964). The oldest recognized glacial deposit and corresponding outwash in

the Truckee basin is the locally named Donner Lake age deposits, followed by the Tahoe age deposits, and finally the youngest Tioga age deposits (Table 1). During the various glacial stages, sediment-laden braided streams aggraded thick sequences of alluvium (fill terraces) that blanketed the bottom of the basin downstream of the corresponding glacial margin, leaving a relatively smooth outwash plain. During deglaciations, these streams incised their channels, leaving prominent terrace risers. Because each successive glaciation was significantly smaller (climatically and spatially) than the previous one (Birkeland, 1964), a nested fill-terrace sequence is preserved in the eastern Truckee basin. Hence, the highest outwash terrace on the basin margins corresponds with the oldest Donner Lake glaciation, and the subsequent Tahoe and Tioga glacial deposits are inset at progressively lower elevations (Birkeland, 1964), as shown in the profile in Figure 3. It is in these deposits that the Polaris fault has geomorphic expression, which is imaged by the high-resolution LiDAR data.

Polaris Fault Characterization

The Polaris fault strikes northwest across the Truckee basin and deforms multiple middle-to-late Pleistocene glacial and fluvial deposits, providing a means to assess important fault characteristics. Our studies focus on three areas that present the most obvious data for evaluating the Polaris fault: (1) the East Martis Creek fan, where the fault is characterized by discontinuous north–northwest (NNW)-trending scarps; (2) the Polaris site, where middle-to-latest Pleistocene terrace risers are right-laterally offset; and (3) the tectonically complex Gray's Crossing site, where the primary northwest-striking Polaris fault right-laterally displaces an early-to-middle Pleistocene terrace riser, a northeast-trending conjugate strike-slip fault left-laterally offsets the same terrace riser, and small thrust faults accommodate north–south shortening along a westerly bend in the Polaris fault (Fig. 1).

Table 1
Stratigraphic Relationships of Selected Quaternary Map Units, Correlation to Marine Oxygen Isotope Stages (If Applicable), and Age Constraints

Map Unit	Marine Oxygen Isotope Stages (MIS) and Age Estimates (ka)
Qtio—Tioga outwash	MIS 2 (13–32) * $>14.0^{\dagger}$ to $<25.2 \pm 2.5^{\ddagger}$
Qtao—Tahoe outwash	MIS 4 (64–75) *§ $>62.0 \pm 3.1^{\parallel}$ $\sim 70 \pm 5^{\S}$ 64.0 ± 3.5 to $76.4 \pm 3.8^{\#}$
Qdl—Donner Lake glacial deposits	≥MIS 6? (128–195)* >131**
Qdlo—Donner Lake outwash	~400 to 600††
Qpc—Prosser Creek alluvium	≤1.3 Ma‡‡

*Shackelton and Opdyke (1976).
†Clark and Gillespie (1997).
‡Bursik and Gillespie (1993).
§Gillespie (1991).
‖Howle *et al.* (2005).
#James *et al.* (2002).
**Yount and La Pointe (1997).
††Birkeland (1964).
‡‡Birkeland (1963).

East Martis Creek Fan

The East Martis Creek fan is located ~2.5 km south of Martis Creek Dam. Sylvester *et al.* (2007) has mapped the fan as Holocene alluvium, while I. Wong *et al.* (unpublished report, 2008, see Data and Resources) suggest that the fan is late Pleistocene in age based on the relative stratigraphic position (Figs. 1, 4, and 5). Initial inspection of the LiDAR data revealed a linear feature that cuts across the alluvial fan and continues in bedrock for at least 2 km to the south. At the head of the fan, the fault is expressed as a set of discontinuous, west–southwest-facing scarps aligned in a NNW orientation (Figs. 4 and 5). The scarps project northwest through a closed depression and linear graben. At the closed depression, the fault splays and the subparallel fault strands diverge along strike, bounding a linear graben. The eastern strand displays down to the southwest separation, where it projects southeast across the head of the East Martis Creek fan in the vicinity of small thermal springs and seeps. Near the northwestern end of the graben, springs discharge from both fault strands (Figs. 4 and 5). Over the length of the graben, the western strand displays down to the northeast morphology and projects northwest through a narrow topographic notch and across Martis Creek Reservoir toward the Martis Creek Dam and spillway (Figs. 4 and 5).

In the fall of 2008, the main fault strand at the head of the fan and the lower fault strand with the prominent vegetation lineament (Fig. 4) were trenched in a paleoseismic investigation (see Fig. 5 for trench locations). Both trenches exposed faults revealing thickening of the stratigraphy across the fault, which is interpreted as indicating strike-slip displacement (Crampton *et al.*, 2009 and Hunter *et al.*, 2009 trench logs). The upper trench documents ~1.5 m of apparent vertical separation from at least three events, while the lower trench revealed ~0.4 m of apparent vertical separation from two events. Structural and stratigraphic relationships in the trenches (near vertical faults at depth that flower near the surface and across fault thickening of the alluvial deposits) are indicative of lateral displacement, but the amount of displacement is unknown. In both trenches, chronologic control was inconclusive; however, in the lower trench, latest Pleistocene to early Holocene alluvium was displaced.

From the graben southeast of Martis Creek reservoir (trending northwest across the reservoir bottom), the only geomorphic evidence of the fault is a broad swale (Fig. 4) that is roughly aligned with the next geomorphic expression of the fault between the western abutment of the dam just north of the spillway. Here, a lineament exposed in the Donner Lake outwash terrace is on strike with the lineament

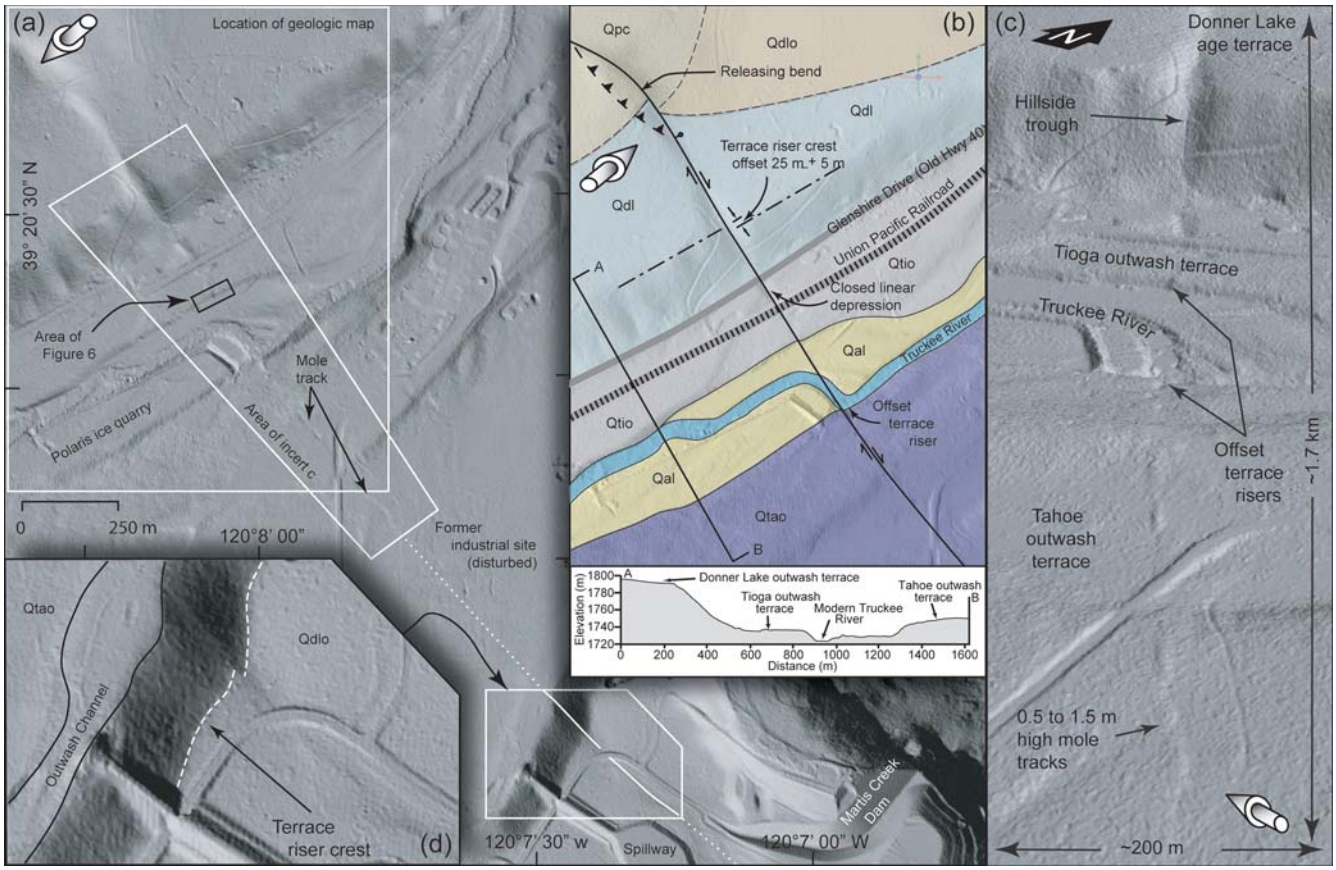

Figure 3. (a) Plan view bare-earth LiDAR image extending from the Martis Creek Dam spillway to the Polaris site (vertical exaggeration is 2). White boxes show the locations of insets (b, c, and d), and black box shows location of Figure 6. The shaded-gray arrow indicates illumination angle. (b) Geologic map modified from Birkeland (1964) superimposed on a LiDAR image. Map units: Qal, Holocene alluvium undifferentiated; Qtio, Tioga age glacial outwash; Qtao, Tahoe age glacial outwash; Qdl, Donner Lake age ground moraine; Qdlo, Donner lake age glacial outwash; Qpc, Prosser Creek alluvium, see Table 1 for ages. Solid lines in (a) and (b) are mapped fault traces (dashed where approximately located, dotted where inferred, barbs on up-thrown side, ball and bar on down-dropped side). Also shown are fault related geomorphic features and selected geographic features. Profile A-B shows the nested relationship of Late Pleistocene fill terraces. (c) Oblique aerial view of bare-earth LiDAR imagery showing along strike fault-related geomorphic features through the Polaris site. View is looking northwest. (d) High-resolution enlargement of subtle scarp cutting across Donner Lake–age glacial outwash terrace and terrace riser, as well as offset terrace riser crest.

southeast of the reservoir (Figs. 3 and 4). A northwest-striking down to the southwest scarp cuts the flat-lying terrace before crossing down the ~38-m-high terrace riser to the Tahoe age outwash terrace (Fig. 3d). From the base of the Donner Lake terrace riser, along strike to the northwest, the trace of the fault is obscured for ~400 m where it passes through a former industrial site that has been graded. Northwest of this disturbed area, approaching the Polaris site, the fault is expressed as a 450-m-long linear mole track (Fig. 3a,c). This narrow linear feature stands 0.5–1.5 m above the smooth Tahoe outwash surface and is probably a product of coseismic deformation of the outwash alluvium.

Polaris Site

At the Polaris site (Figs. 1 and 3), the modern Truckee River is flanked by a Tioga-age glacial outwash terrace on the north side and Tahoe-age outwash terrace on the south side (Birkeland, 1964). These fill terraces have been incised by glacial melt water that formed linear fluvial terrace risers (Fig. 3b). The Polaris fault orthogonally offsets the terrace risers on both the northern and southern sides of the Truckee River in a right-lateral sense. The modern Truckee River is right-laterally deflected to the southeast, along the trace of the fault, and has eroded the offset terrace risers on the south side of the river, modifying the tectonic morphology and thus negating a reliable strain analysis. However, on the north side of the Truckee River, the offset terrace riser has been largely unaffected by Holocene stream processes. At this site, we utilize the relatively pristine morphology and a maximum age of the terrace to estimate a minimum tectonic slip rate.

Using Offset Terrace Risers to Determine a Slip Rate. Because of their simple geometry, offset fluvial terrace risers are one of the most common landforms used to determine rates of strike-slip faulting (Harkins and Kirby, 2008; Gold *et al.*,

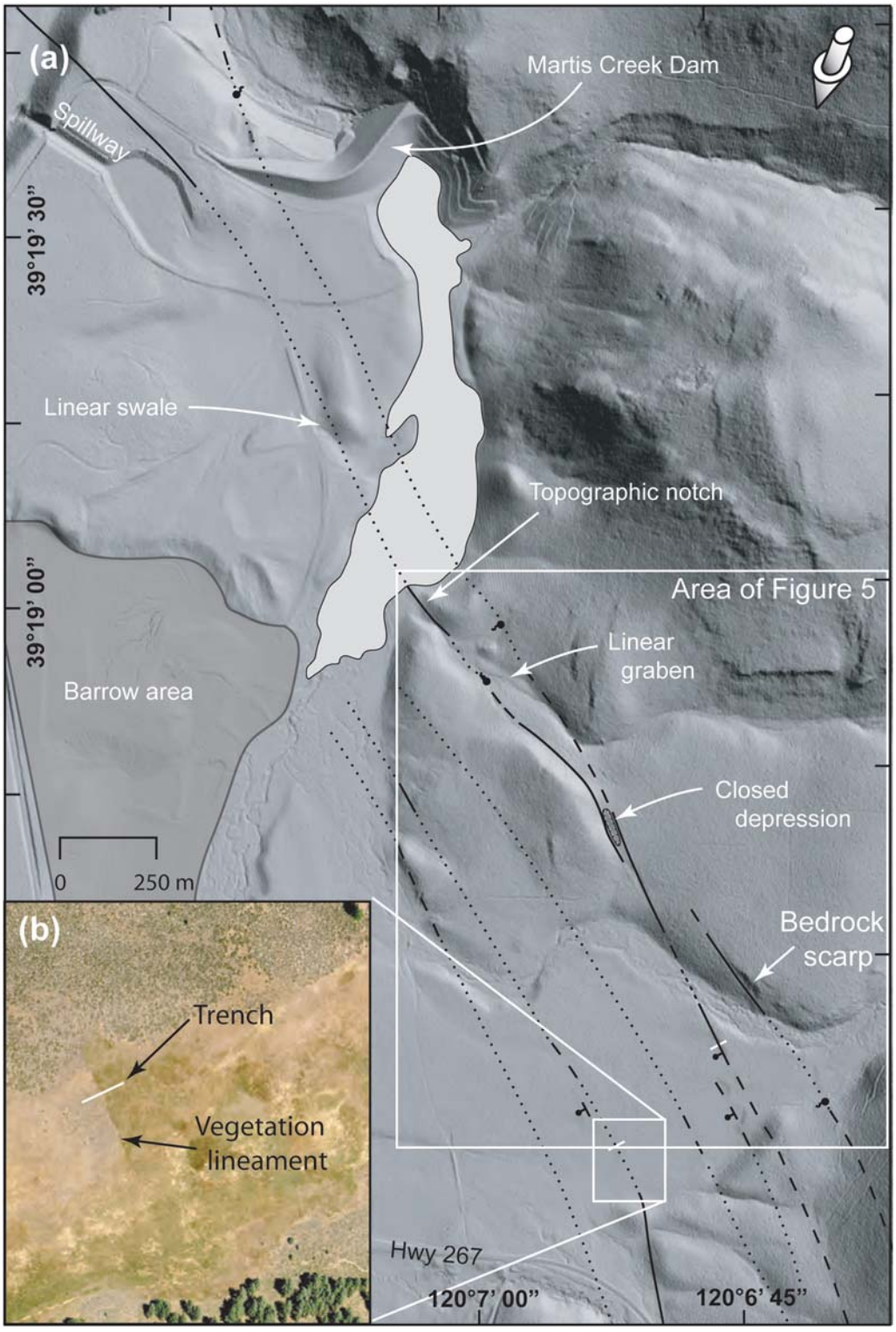

Figure 4. (a) Plan-view bare-earth LiDAR image, extending from the East Martis Creek fan to the Martis Creek Dam spillway (vertical exaggeration is 2). See Figure 1 for regional location. Gray-shaded arrow (upper right) indicates direction of illumination. Also shown are mapped fault traces (dashed where approximately located, dotted where inferred, ball-and-bar on down-dropped side), as well as fault-related geomorphic and hydrologic features described in the text. Locations of two paleoseismic trenches are depicted by thin white lines, and white boxes show the area of inset (b) and Figure 5. (b) Plan-view aerial photograph, showing vegetation lineament on south side of the East Martis Creek fan and location of trench (see text and Fig. 5).

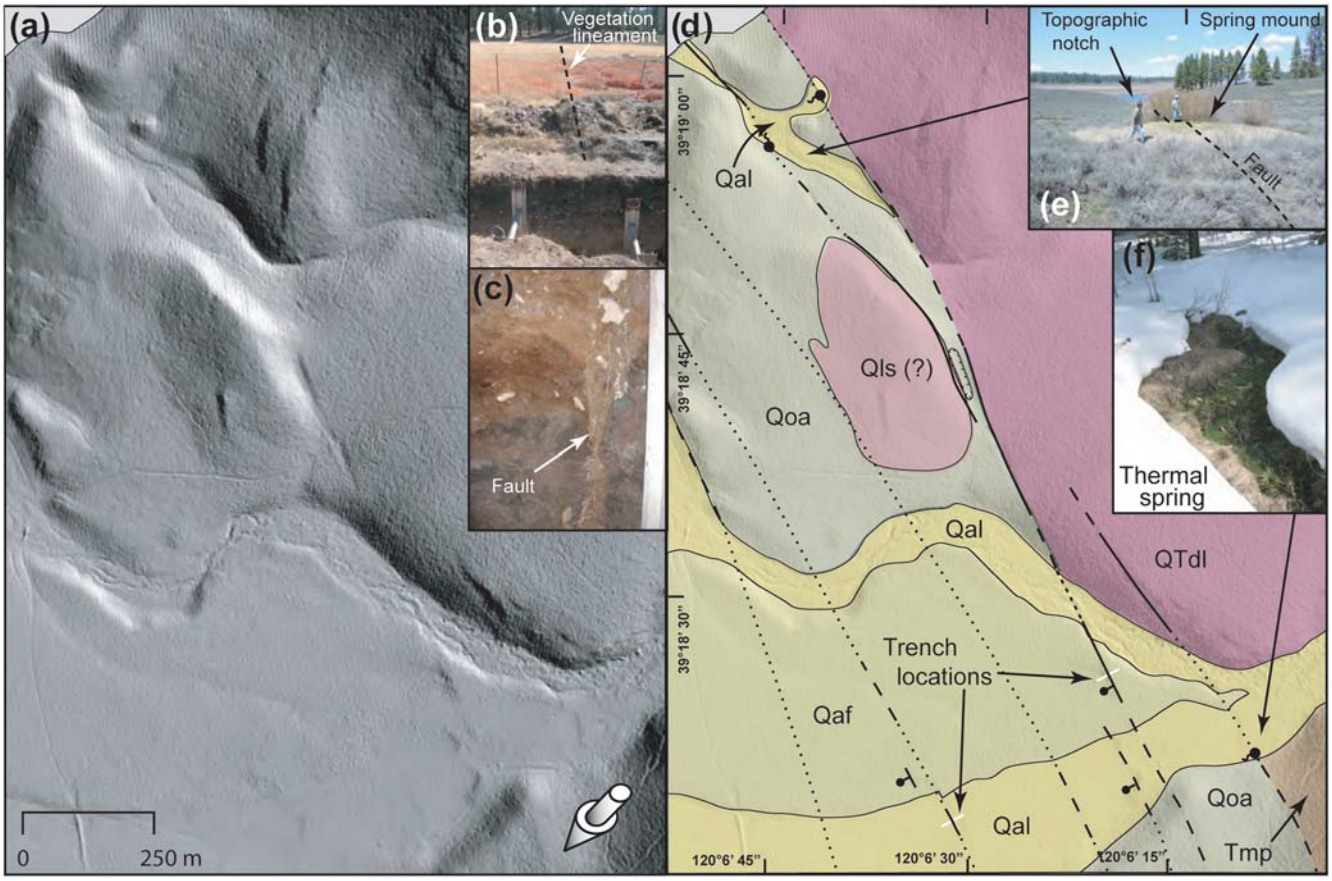

Figure 5. (a) Plan-view bare-earth LiDAR image of the East Martis Creek fan (vertical exaggeration is 2). Gray-shaded arrow indicates direction of illumination. (b) View of vegetation lineament on fan surface in background and trench in foreground. (c) Vertical fault exposed in trench and aligned with vegetation lineament on fan surface. Aluminum shoring on the right side of insets (b) and (c) are the same. (d) Geologic map (modified from Sylvester *et al.*, 2007, and Crampton *et al.*, 2009) superimposed on LiDAR image. Qal, Holocene alluvium undifferentiated; Qaf, alluvial fan deposits (see text for age discussion); Qoa, dissected older alluvium; Qls, landslide deposit; QTdl, Dry Lake andesitic flows; Tmp, Martis Peak pyroclastic andesite. Solid black lines are mapped fault traces (dashed where approximately located, dotted where inferred, ball and bar on down-dropped side). Photograph insets: (e) spring mound located on fault trace at northwest end of linear graben and (f) thermal spring near the head of the East Martis Creek fan.

2009, and references therein). "Determining a rate of strike-slip faulting is simple in principle because only two measurements are needed: a magnitude of offset and the time over which this displacement accrued" (Cowgill, 2007, p. 240). The terrace riser genesis is described in the next paragraph, and the underlying assumptions for using the offset Tioga-age terrace risers as a geomorphic strain marker are listed in the following section (Geomorphic Criteria for Using Offset Terrace Risers as Strain Markers).

First, aggradation of the Tioga-age glacial outwash terrace (fill terrace) occurred during the glaciation due to glacial quarrying that increased the sediment flux, as well as increasing the sediment size (i.e., cobbles and boulders) to the proglacial stream (Birkeland, 1964 and Hallet *et al.*, 1996). Subsequently, deglaciation melt water increased the stream discharge while, at the same time, sediment size and flux decreased, causing the stream to incise the risers and abandon the terrace (Birkeland, 1964 and Repka *et al.*, 1997). Thus, we assume that the terrace riser formed by the end of the Tioga deglaciation and that the abandonment age of the Tioga outwash terrace represents a maximum limiting age of the tectonic displacement (i.e., the riser formed first, followed by tectonic displacement).

Age of Offset Tioga Deposit. In the central Sierra Nevada, the Tioga deglaciation is constrained at 14.5 ± 0.5 ka, based on radiocarbon dating of basal sediments impounded by terminal moraines (Clark and Gillespie, 1997). In the northern Sierra Nevada, 35 km west of the Polaris site, James *et al.* (2002) demonstrate that the Tioga deglaciation occurred by 14.1 ± 1.5 ka, using cosmogenic beryllium-10 (^{10}Be) exposure dating of a glacially striated bedrock valley. Benson *et al.* (1990) provide detailed radiocarbon data constraining fluctuations of Pleistocene Lake Lahontan. These data, specific to the Truckee River drainage, suggest that locally the Tioga deglaciation may have ended at 13.3 ± 0.3 ka. Based on these studies, we consider the maximum age of the terrace riser to be 14 ± 1.5 ka (i.e., the maximum limiting age of tectonic displacement). This scenario of constraining the slip rate with a maximum limiting age or an upper terrace

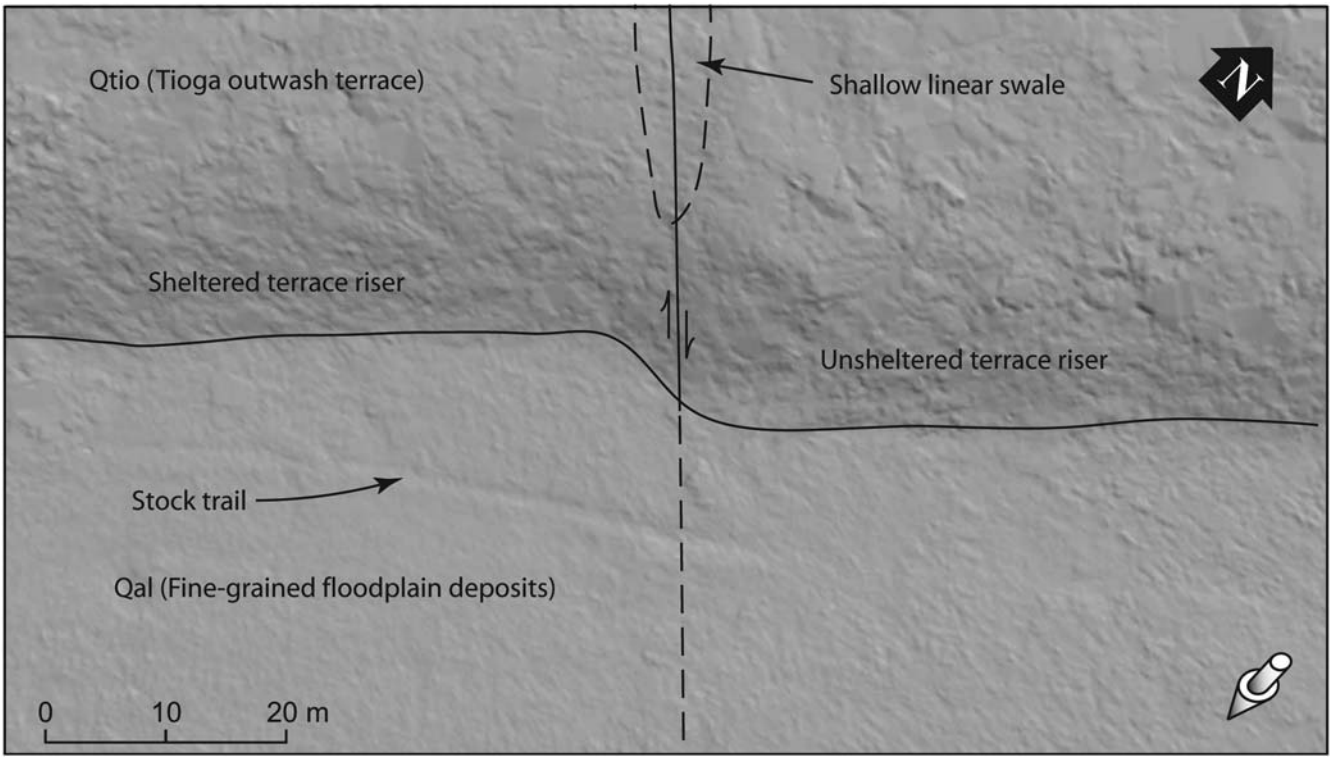

Figure 6. Plan-view bare-earth T-LiDAR image of offset Tioga-age terrace riser at the Polaris site, showing the linear and parallel offset terrace risers on either side of the fault trace and abrupt truncation of the risers in a narrow fault zone. See Figure 3 for location. There is no vertical exaggeration. Shaded-gray arrow indicates illumination angle.

reconstruction produces a conservative minimum slip rate estimate (Cowgill, 2007; Gold *et al.*, 2009).

Geomorphic Criteria for Using Offset Terrace Risers as Strain Markers. At the Polaris site, the modestly degraded morphology of the Tioga terrace riser is attributed to the youthful age that makes this locality well suited as a geomorphic strain marker. Geomorphic criteria that support the use of these offset risers as a strain marker are: (1) The offset terrace risers are linear for ~60 m on either side of the fault. (2) The terrace risers are abruptly and orthogonally truncated in a narrow fault zone ~10 m wide. (3) The riser faces (planar section below the degraded riser crest and above the colluvial wedge at the base) on either side of the fault are nearly parallel (strikes differ by $< 6°$) and have very similar dips (dips vary by 1–1.5°). 4) Across-fault correlation of terrace risers is straightforward because there is only one on either side, they are equal in height on either side of the fault, and the curvature of the degraded riser crests are similar. In addition, we assume that no Holocene lateral erosion of the risers has occurred because the modern Truckee River flows away from the offset riser (Fig. 3). Furthermore, during major flood events, relatively slow and weak overbank flow has deposited a veneer of fine sand and silt that has partially buried the colluvial wedge at the base of the terrace riser rather than eroding the riser base. If the unsheltered riser (downstream riser nearest the active channel) were laterally eroded by Holocene stream processes, then the magnitude of the displacement would be reduced, further making the slip rate estimate a minimum.

Reconstructing Offset Terrace Risers. Displacements of fluvial terrace risers are usually reconstructed in a two-dimensional (2D) plan-view map from total station and/or GPS survey data (e.g., Cowgill, 2007; Harkins and Kirby, 2008). Surveyed points typically represent field interpretations of the riser crest and/or base location that are best fit to a line, which is then projected to an intersection with the fault trace to determine piercing points on a plan-view map. Uncertainties in the cumulative displacement associated with this type of 2D reconstruction range from 3 to 7 m (Cowgill, 2007; Harkins and Kirby 2008; Gold *et al.*, 2009).

At the Polaris site, Howle *et al.* (2009) utilized high-resolution ground-based LiDAR imagery of the offset terrace risers (Fig. 6) to mathematically reconstruct pristine terrace–scarp morphologies on both sides of the fault, define coupled sets of piercing points, and extract a corresponding displacement vector (Fig. 7). By using ground-based or terrestrial LiDAR (T-LiDAR), thousands of points per square meter were collected over an $\sim 12,000\text{-m}^2$ area surrounding the offset terrace risers. Vegetation was removed from the point-cloud data using TerraScan software (see Data and Resources section) and large protruding boulders were manually deleted to generate a bare-earth point-cloud dataset with an average data density of over 240 points per square meter.

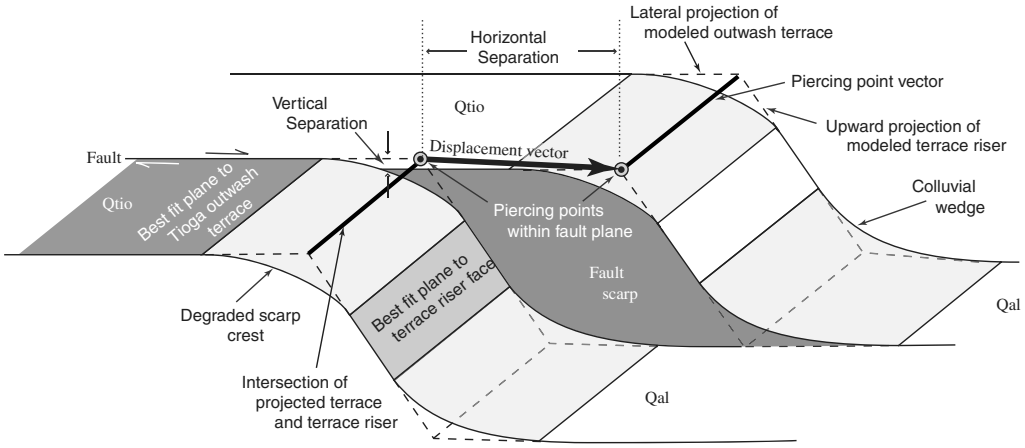

Figure 7. Oblique schematic of offset terrace riser depicting the mathematical 3D reconstruction used to define piercing points and to extract a corresponding displacement vector. See text for discussion. (Figure is not to scale.)

The orientation of the Polaris fault was approximated in the 3D data as a vertical plane that bisects the offset terrace risers, as well as linear swales and tectonic depressions along strike in the Tioga outwash terrace. Using the 3D T-LiDAR image, piercing points to the vertical fault plane were mathematically extracted from the geometry of the geomorphic elements on either side of the fault. On each side of the fault, equal area planes were best fit (with a linear regression) to the outwash terrace as well as the terrace riser face, excluding points on the degraded scarp crest and colluvial wedge at the riser base (Fig. 7). Then, on each side of the fault, the model outwash terrace plane was projected laterally and the modeled terrace riser face was projected upward to a virtual intersection, creating vectors. These constructed vectors were projected to an intersection with the fault plane, defining statistically significant piercing points. The distance between the coupled set of piercing points, within the plane of the fault, yields the cumulative displacement vector (Fig. 7).

To assess the variability of the modeled tectonic displacement due to surface roughness and nonlinearity of the landform, Howle *et al.* (2009) generated a suite of ten displacement models by systematically incorporating larger areas into the model domain symmetrically about the fault. The area modeled for individual outwash terraces on either side of the fault ranged from 800 m^2 to 2200 m^2, and the area modeled for individual terrace risers ranged from 240 m^2 to 440 m^2. On average, for the ten displacement models, 95% of the point cloud (laser ground points) was within ± 0.06 m of the best-fit modeled plane.

This numerically robust technique has the statistical advantage of integrating hundreds of thousands of data points collected over a broad area, which collectively yield the cumulative displacement vector. The total number of ground points used to constrain the displacement vectors in the ten models ranges from over 163,000 to nearly 303,000. Results of the ten displacement models yields an average cumulative displacement of 5.6 m (1 Std Dev = 0.31 m). The 3D modeling reveals a small down to the east component of displacement that is not readily apparent in the field. The average ratio of horizontal-to-vertical displacement at this site is ~12:1. However, this is not a far-field strain (i.e., not representative of regional transtention) but rather a localized feature related to a releasing bend along the Polaris fault (see discussion in the section Progressive Deformation at the Polaris Site).

Using the 5.6 ± 0.3 m of cumulative displacement and the maximum limiting age of 14 ± 1.5 ka discussed previously in this article, Howle *et al.* (2009) estimate a preliminary minimum fault slip rate of 0.4 ± 0.1 mm/yr for the Polaris site since the Pleistocene–Holocene boundary. While this estimate is not a long-term time-averaged rate, it currently represents the only slip-rate estimate for the Polaris fault.

Progressive Deformation at the Polaris Site. Along strike, 300 m northwest of the Tioga-age offset, there is a larger dextral offset of an ~35-m-high terrace riser (Fig. 3) eroded into middle(?)-Pleistocene Donner Lake ground moraine. Because of the large uncertainties in the absolute age of the Donner Lake age deposits (Table 1), no slip rate estimate is inferred here. However, the scarp crest and terrace riser are right-laterally offset by 25 ± 5 m, demonstrating progressive deformation relative to the post-Tioga offset. In addition, ~5 m of down to the east displacement is observed in the relatively flat upper terrace of Donner Lake ground moraine (Fig. 3).

In between these offset scarp crests, the fault is expressed as an anomalously deep and broad hillside trough that has no appreciable colluvium at the base but rather a closed linear depression (Figs. 3 and 8). These anomalous features and the previously mentioned down to the east displacement are interpreted as being caused by collapse of the unconsolidated deposits into the fault zone along a releasing bend in the fault. Just north of this hillside trough is a westerly bend in the fault trace (Figs. 3 and 8). Along the convex east side of the bend (releasing bend), right-lateral displacement opens a void, creating a localized zone of extension that allows for the collapse of unconsolidated deposits into the

fault zone and produces oblique normal separation of the Donner Lake terrace. Conversely, on the concave west side of the bend (restraining bend), right-lateral displacement creates a localized zone of shortening, highlighted here by an elongated contractional ridge in the Prosser Creek alluvium, which we interpret to be a product of a shallow-thrust fault.

The Gray's Crossing Site

The Gray's Crossing site is located approximately 2.5 km northwest of the Polaris site and 4 km northeast of Truckee, California (Figs. 1, 8, and 9). The site is on a relatively flat upland surface comprised of early-Pleistocene Prosser Creek alluvium, which is thought to be coeval with the 1.3-Ma Hirschdale basalt (Birkeland, 1963; Sylvester *et al.*, 2007). Incised into the Prosser Creek alluvium is a linear north–northeast-trending paleochannel (Figs. 8 and 9) mantled with Donner Lake–age outwash, indicating the abandoned channel was cut during the Donner Lake glaciation (Birkeland, 1964).

At the Gray's Crossing site (Figs. 8 and 9), the airborne LiDAR imagery reveals a prominent west–northwest (WNW)-trending lineament that is expressed as a series of aligned, elongated depressions (as much as 4 m deep) and linear mounds up to 5 m high (mole tracks). These features could be the result of small-scale fault-plane undulations where releasing bends create depressions and restraining bends cause contraction, forming the linear mounds. Of special interest are (1) the offset terrace risers along the western side of the paleochannel (Fig. 9), where the northwest-striking Polaris fault right-laterally offsets the fluvial terrace riser by 58 ± 4 m, and (2) to the south is a 43 ± 5 m left-lateral offset of the same terrace riser on a northeast-trending conjugate strike-slip fault (Fig. 9). Because of the large uncertainties in the absolute ages of the upper-terrace Prosser Creek alluvium (age based on stratigraphic correlation) and the lower Donner Lake outwash (Table 1), no slip rate estimates are inferred at this site. I. Wong *et al.* (unpublished report, 2008, plate 2; see Data and Resources) recognize this conjugate lineament and depict it in the southwestern corner of the broadly distributed and discontinuous Dog Valley fault zone (DVFZ in Fig. 1a).

The Gray's Crossing site lies at the western end of an ~2-km-long section of the Polaris fault that strikes more westerly than northwesterly (Figs. 1 and 8). Right-lateral motion creates a localized zone of contraction along this bend in the Polaris fault. Localized shortening is evident in the north and

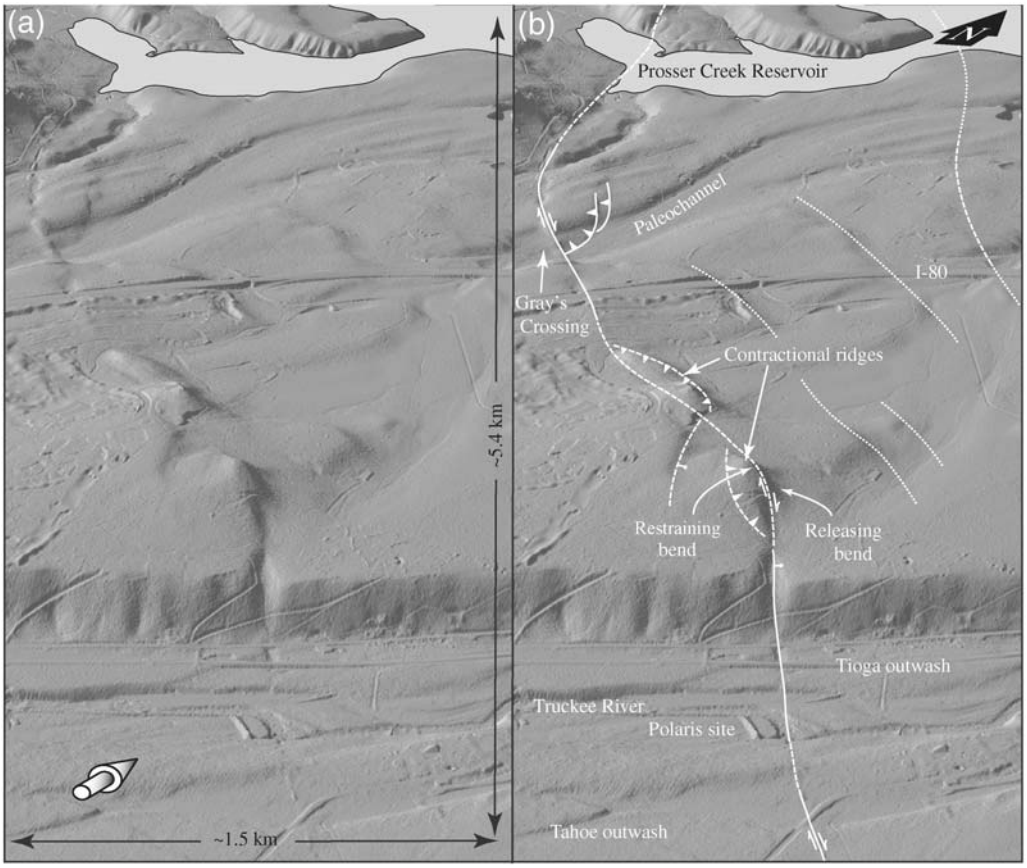

Figure 8. (a) Oblique aerial view of bare-earth LiDAR imagery, extending from the Polaris site to Prosser Creek Reservoir. (View is looking to the northwest.) Shaded-gray arrow indicates illumination angle (vertical exaggeration is 2). (b) Solid white lines are mapped fault traces (dashed where approximately located, dotted where inferred, barbs on up-thrown side, ball and bar on down-dropped side). Also shown are fault-related geomorphic features and selected geographic features. See text for discussion of releasing and constraining bends.

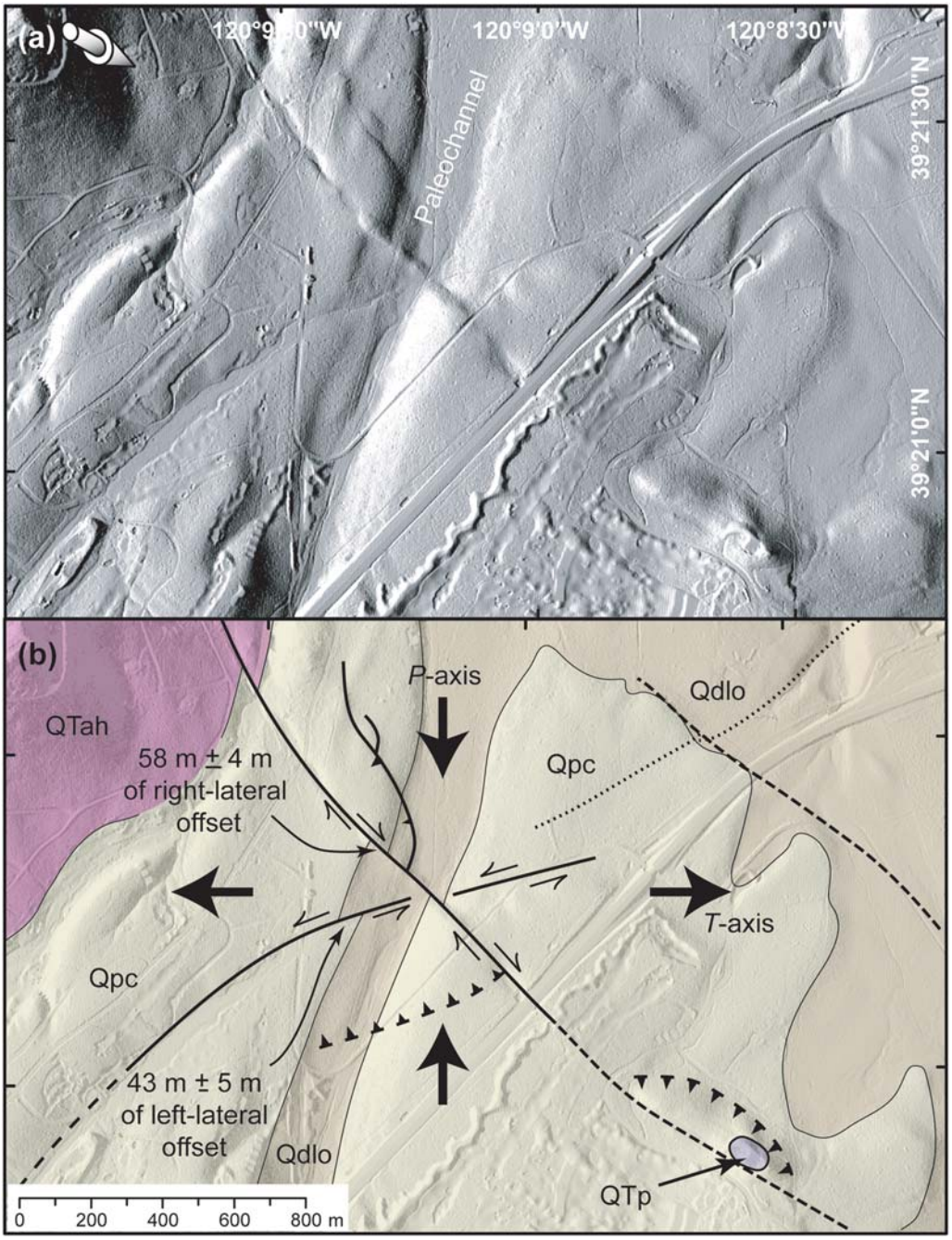

Figure 9. (a) Plan-view bare-earth LiDAR imagery of the Gray's Crossing site. Shaded-gray arrow indicates illumination angle (vertical exaggeration is 2). (b) Geologic map modified from Birkeland (1964) and superimposed on a LiDAR image. Map units: Qdlo, Donner Lake age glacial outwash: Qpc, Prosser Creek alluvium; QTp, Polaris basalt; and QTah, Alder Creek olivine basalt. Solid black lines are mapped fault traces (dashed where approximately located, dotted where inferred, barbs on up-thrown side), and bold arrows indicating the orientation of the maximum principal stress (*P*-axis) and minimum principal stress (*T*-axis) vectors. (See text for discussion.)

south quadrants, defined by the intersection of the Polaris fault and its conjugate (Fig. 9). Along the west side of the northern quadrant, an apparent reverse fault is represented by a sharp, arcing topographic lobe that intersects the main fault at almost a right angle before turning to the northwest and extends for several hundred meters in an orientation that is subparallel to the main fault (Fig. 9). In the southern fault-bounded quadrant, just east of the paleochannel, is a conspicuous 5-m-high rise in the otherwise flat-lying Prosser Creek alluvium. We interpret this rise (or fold?) as a product of a blind thrust fault that accommodates the localized north–south contraction.

Northwest of the Gray's Crossing site, the Polaris fault strikes north–northwesterly and is expressed as a 7-m-high northeast-facing scarp coincident with a sharp tonal–vegetation lineament south of Prosser Creek Reservoir (Figs. 8 and 10g). Where Alder Creek enters the southwest

Figure 10. (a) Location map showing plan-view bare-earth LiDAR imagery from Prosser Creek Reservoir to Sagehen Creek northwest of Hobart Meadow. White boxes show the locations of insets (b and c), (d and e), and (g). Bare-earth images have a vertical exaggeration of 2.5, and shaded-gray arrows indicate illumination angle. Solid black lines are mapped fault traces (dashed where approximately located, dotted where inferred, ball and bar on down-dropped side). (b) Enlargement of bare-earth image near Hobart Mills with (c) annotations of features discussed in the text. (d) Enlargement of the bare-earth imagery along the west side of Prosser Creek Reservoir with (e) annotations of features discussed in the text and topographic profile of the scarp in alluvium, showing location of linear seep shown in (f). (g) Aerial photograph showing tonal–vegetation lineament coincident with the fault scarp southwest of Prosser Creek Reservoir. (DVFZ, Dog Valley fault zone; ETFZ, Eastern Truckee fault zone.)

arm of Prosser Creek Reservoir, a fault-shunted ridge right-laterally deflects the course of Alder Creek to the south (Fig. 10d,e). On the south and north sides of the peninsula between the arms of Prosser Creek Reservoir, the Polaris fault is expressed as a set of deeply incised gullies with little or no contributing drainage areas (Fig. 10e). These anomalously deep gullies are aligned with the fault and have preferentially developed along it. Between these conspicuous

drainages is an ~8-m-high northeast-facing scarp in unconsolidated alluvium (see profile in Fig. 10e). Along the base of the scarp is an ~200-m-long linear seep with lush grass surrounded by sage brush (Fig. 10f). Dissecting the peninsula, east of the fault, is a beheaded former channel of Prosser Creek that apparently was abandoned due to right-lateral displacement along the Polaris fault (e.g., Oskin *et al.*, 2007). Along strike to the northwest and southeast of Hobart Mills, the modern course of Prosser Creek is fault-controlled before it enters the northwest arm of Prosser Creek Reservoir (Fig. 10a). Just south of Hobart Mills, the 25-m-high terrace riser flanking the north side of Prosser Creek is dextrally offset ~100 m where the Polaris fault makes a slight bend to the NNW (Fig. 10c). At Hobart Mills is a 400-m-long NNW-striking linear scarp with a spring issuing from the base that is aligned with the offset terrace riser to the south–southeast SSE. Where the scarp projects to the NNW, it is aligned with subtle breaks in slope on intervening ridges and a tonal–vegetation lineament that continues NNW along the linear west side of Hobart Meadow (Fig. 10c).

Complex Zone of Spatially and Kinematically Linked Faults. Between Hobart Mills and Hobart Meadow is a complex zone where three faults with different orientations and senses of displacement intersect (Fig. 10a). Just north of Hobart Mills, the main trace of the northeast-striking left-lateral DVFZ, as mapped by Hawkins *et al.* (1986), abruptly terminates where it intersects the NNW-striking right-lateral Polaris fault on the south side of Billy Hill (Fig. 10a). To the WNW of Hobart Mills, there is an apparent 1.5 km gap in the DVFZ (Hawkins *et al.*, 1986; Olig *et al.*, 2005) before resuming along the northeast-trending reach of Prosser Creek (Fig. 1). Using the high-resolution LiDAR imagery, we interpret that the main trace of the DVFZ is right-laterally offset ~0.9 km by the Polaris fault between Hobart Mills and Hobart Meadow (Fig. 10a,c). Approximately 1 km south of Hobart Meadow and west of Hwy 89, the fault trace resumes and continues for 2 km along the southeast flank of the Sagehen Hills before it rejoins the northeast-trending reach of Prosser Creek, as originally mapped by Hawkins *et al.* (1986).

At Hobart Meadow, the Polaris fault intersects the Eastern Truckee fault zone (ETFZ in Figs. 1a and 10). To the south of this intersection, the ETFZ has been mapped (Birkeland, 1963; Latham, 1985) as a down to the east normal fault evidenced by ~200-m-high triangular facets on the eastern side of Alder and Prosser Hills (Fig. 10a). However, at Hobart Meadow, the strike and sense of displacement of the ETFZ changes from a north-striking down to the east normal fault to a NNW-striking fault with dextral features (Figs. 10 and 11).

Hobart Meadow is a triangular-shaped fault-bounded closed depression and forms a prominent saddle on the topographic divide between Prosser and Sagehen Creeks. A paleoseismic trench at Hobart Meadow (Melody, 2009) documents a north-striking normal fault with ~1 m of down to the east vertical separation. Radiocarbon dating constrains one and possibly two Holocene events (<7 ka). This data demonstrate the recency of faulting in this complex zone of intersecting faults bounding the closed depression.

Tectonic Geomorphology along the Northern Extent of the Polaris Fault. From Hobart Meadow NNW to Kyburz Flat, the ETFZ as mapped by Olig *et al.* (2005) is mostly coincident with our mapping. Along this northern section, the fault leaves the Pleistocene deposits of the Truckee basin and traverses Tertiary volcanic bedrock, where it is primarily expressed as larger scale offsets and alignments of creeks and rivers (I. Wong *et al.*, unpublished report, 2008, see Data and Resources).

Northwest of Hobart Meadow, the general west-to-east trend of Sagehen Creek is offset ~1.6 km to the southeast along a fault-controlled reach on trend with the Polaris fault (Figs. 11 and 12). To the north, this lineament projects through a bedrock notch and another prominent ridge-crest saddle where Highway 89 crosses Sagehen Summit (Fig. 12). North of Sagehen Summit, the west-to-east trend of the Little Truckee River is similarly right-laterally offset for ~5 km along a NNW-trending reach (Fig. 11). The offsets and alignment of Sagehen Creek and the Little Truckee River along a NNW trend was originally recognized by William Page (cited as a written communication circa 1995 in Olig *et al.*, 2005). Along the northwest-trending reach of the Little Truckee River, I. Wong *et al.*, (unpublished report, 2008, see Data and Resources) retrodeform 5 km of right-lateral displacement based on a planimetric reconstruction of an east–west trending andesite–basalt contact, which is roughly coincident with the offset east-flowing reaches of the Little Truckee River to the northwest and southeast (Fig. 11). Along this reach of the Little Truckee River north of Sagehen Summit to Kyburz Flat are conspicuous NNW-striking geomorphic features, such as linear valley edges and linear ridges. Just north of Sagehen Summit is a narrow linear graben that is over 80 m deep with only a minor stream draining it to the north (Fig. 12). On the west side of this triangular-shaped valley is the beginning of a fault-bounded hillside bench that continues for 4 km to the NNW above the Little Truckee River valley. Near the northern end of this linear hillside bench and 45 m above the river is a small thermal spring that flows from the mapped fault trace (Fig. 12).

Where the Little Truckee River turns east and exits the northwest-trending reach, the channel character changes from a sediment-choked braided channel to a narrow bedrock channel coincident with a mapped fault trace (Fig. 12). The ponding of sediment, upstream of the mapped fault trace, can be explained by right-lateral displacement (possibly right oblique) where bedrock on the east side of the fault is shunted across the active channel, damming the river and effectively raising the bedrock sill. A right-lateral component along this mapped fault trace is demonstrated by the right-lateral deflection the Little Truckee River and the right-lateral offset of the Sagehen Creek valley to the south. Here, on the north side of

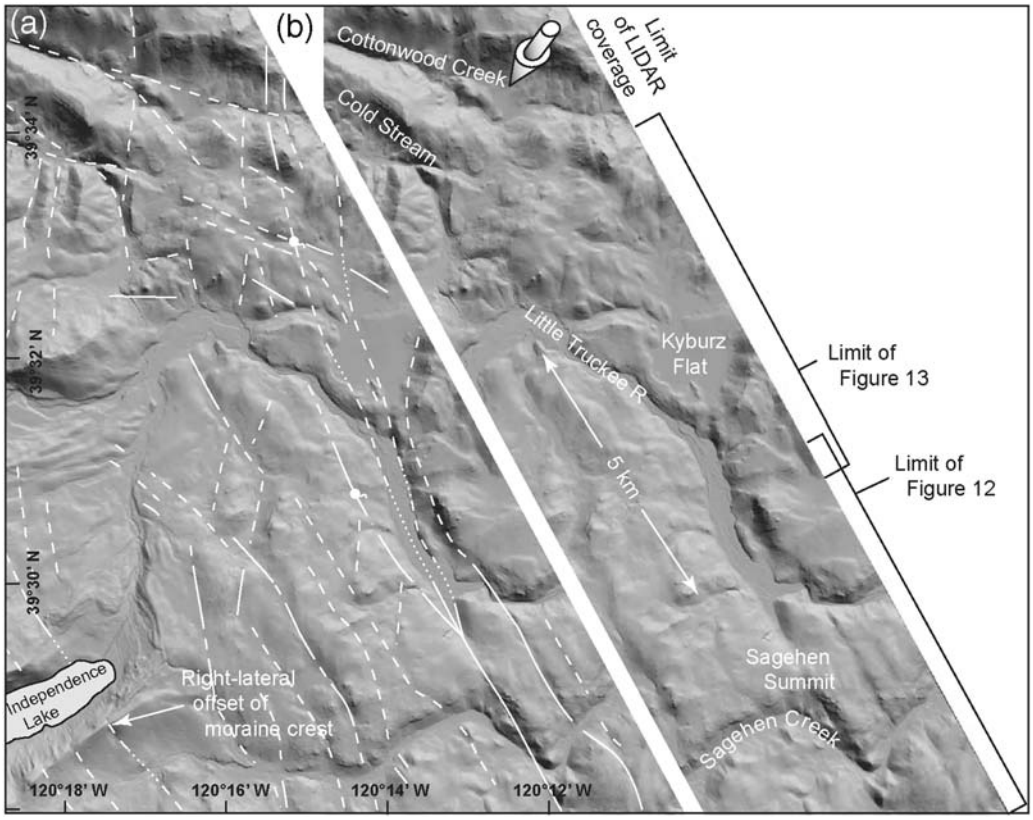

Figure 11. (a) Plan-view bare-earth LiDAR image showing overview of structural interpretations from Sagehen Creek to Cottonwood Creek. Shaded-gray arrow indicates direction of illumination (vertical exaggeration 2.5). (b) Geographic features described in the text, and northwest to southeast extent of Figures 12 and 13.

Sagehen Creek, the linear valley edge and valley wall is right-laterally juxtaposed. In addition, this northeast-trending reach of Sagehen Creek appears to be a left-lateral structure. Sinistral motion is inferred here by the northeast orientation of the linear drainage and the opposing bedrock scarps along the northwest-striking dextral fault on either side of Sagehen Creek. Left-lateral motion would induce a down to the southwest normal component north of the creek and down to the northeast normal component south of the creek, as highlighted by the illumination in Figure 12.

Collectively, these geomorphic, geologic, and hydrologic observations from Kyburz Flat to Hobart Meadow strongly suggest a structural connection with the Polaris fault to the southeast.

Distributed Nature of Faulting along the Northern Extent of the Polaris Fault. At Sagehen Summit, the Polaris fault splays with the western strand, continuing NNW, and the subparallel eastern strands striking more northerly towards Kyburz Flat, where they diverge to the north and northeast (Figs. 11, 12, and 13). The western strands display east down normal components, and the eastern strands have west down normal components, creating an extensional trough. This scenario of a splaying strike-slip fault with inward-facing normal components is an example of extensional or negative flower structure. This fault-bounded extensional trough helps explain the wide underfit appearance of the Little Truckee River along the ~5 km NNW-trending reach.

The complex nature of the faulting at the northern end of the Polaris fault (i.e., a strike-slip fault splaying into normal faults) is noted elsewhere in the NWL, where dextral strike-slip faults are observed to end in arrays of north-striking normal faults (Faulds *et al.*, 2005; Faulds and Henry, 2008) that are similar to both the northern and southern ends of the Polaris fault.

Local Fault Patterns Relative to Regional Tectonics

At the latitude of the Truckee basin, the Polaris fault and subparallel strands (described in the following section) represent the westernmost dextral structures of the NWL. The Polaris fault fills a recognized ~35-km-long gap between the Mohawk Valley fault zone (MVFZ in Figs. 1 and 2) to the northwest and Lake Tahoe basin faults to the south (S. Olig *et al.*, unpublished report, 2005, see Data and Resources). Together, the ~85-km-long MVFZ (Page *et al.*, 1993; Olig *et al.*, 2005) and the Polaris fault define an ~120-km-long zone of dextral faults in the westernmost part of the NWL.

Throughout the NWL, where dextral strike-slip faults end, they are commonly observed to make en echelon left-steps to adjacent strike-slip faults (Faulds *et al.*, 2005;

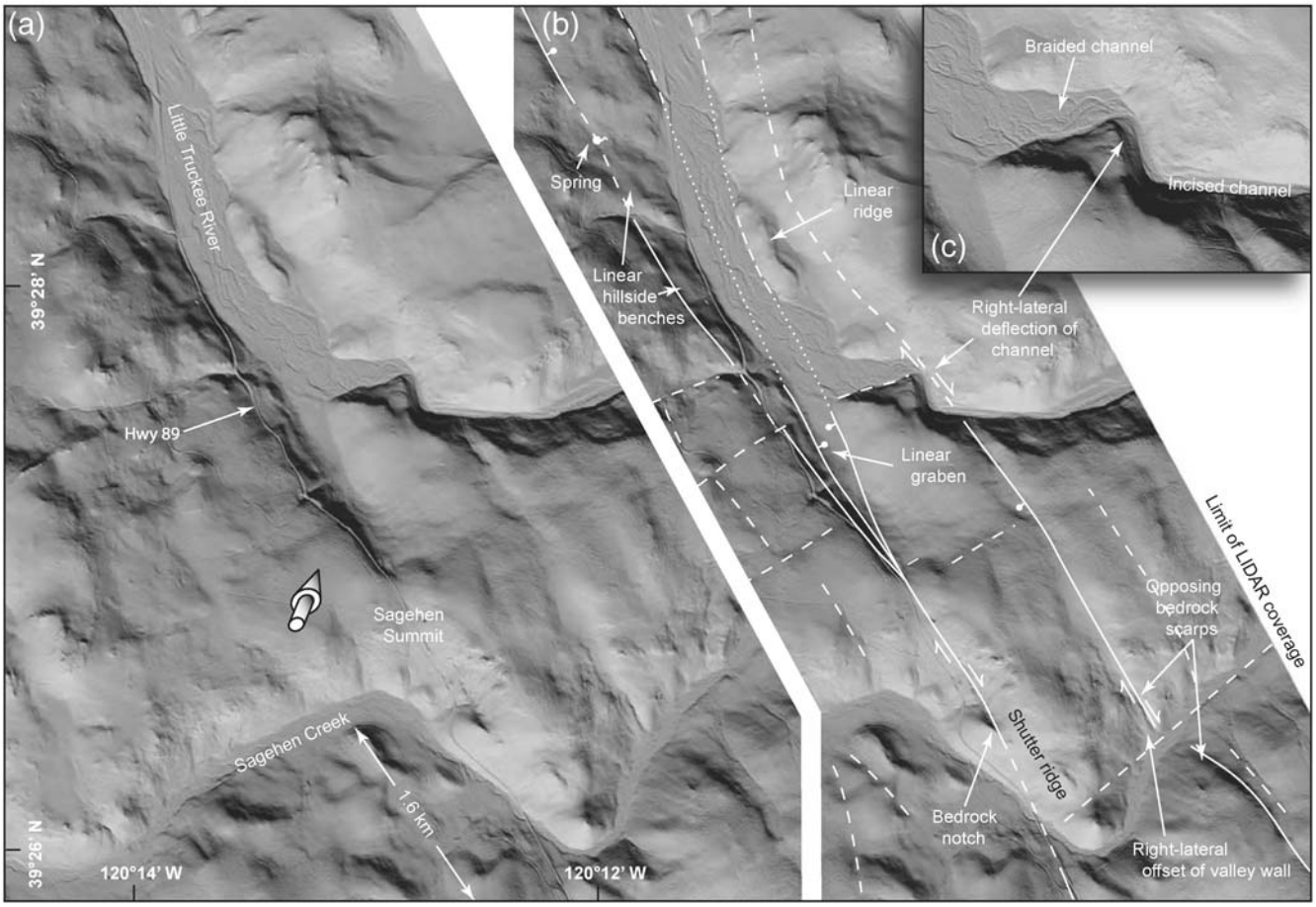

Figure 12. (a) Plan-view bare-earth LiDAR image of the area near Sagehen Summit and selected geographic features. Shaded-gray arrow indicates direction of illumination (vertical exaggeration 2.5). (b) Solid white lines are mapped fault traces (dashed where approximately located, dotted where inferred, ball and bar on down-dropped side). Also shown are fault-related geomorphic features described in the text. (c) Detailed inset showing right-lateral offset of channel coincident with mapped fault and change from braided channel to incised bedrock channel.

Faulds and Henry, 2008). However, the structural connection between the MVFZ and the Polaris fault is notably different. In this case, the MVFZ and Polaris fault appear to intersect at about 45° in a structurally complex zone between the Sierra Valley and Kyburz Flat (Fig. 1). At the northern extent of the Polaris fault, north of Kyburz Flat, the mapped NNW lineaments die out where they intersect topographically strong WNW-trending lineaments at the head waters of Cottonwood and Cold Stream Creeks (Fig. 11). These lineaments projecting out of the Sierra Valley to the SSE are the southeastern-most mapped structures of the MVFZ (Sawyer *et al.*, 1995; Grose, 2000; Sawyer and Briggs, 2001; Sawyer *et al.*, 2005), and where they die out is only 5 km from Kyburz Flat. This structurally complex zone between the Sierra Valley and Kyburz Flat is dissected by short NNW-trending lineaments that are crosscut by pervasive WNW-trending lineaments forming northwest-oriented rhombohedral shaped blocks on the scale of a few hundred meters up to ~2 km in length (Figs. 11 and 13). The northwest alignment of the Little Truckee River immediately west of Kyburz Flat and the southeastward projection of the linear headwaters of Cold Stream and Cottonwood Creek (Figs. 1b and 11) are suggestive of an incipient through-going structure. Because this part of the NWL is the youngest (Faulds *et al.*, 2005; Faulds and Henry, 2008) and least well developed (Wesnousky, 2005a, 2005b), this possible connection between the MVFZ and Polaris fault is structurally immature, and it is unclear how strain is partitioned across it.

In the MVFZ to the northwest and Honey Lake fault zone to the northeast (HLF in Fig. 2b), as well as numerous other locations throughout the Walker Lane and ECSZ (Fig. 2a), regional dextral shear is partitioned across subparallel faults. At these locations the western strands form range-front normal faults (accommodating localized extension approximately perpendicular to the range front; Ichinose *et al.*, 2003), and the more active eastern strands are dextral strike-slip faults that accommodate Pacific–North American plate boundary-related shear (Wesnousky and Jones, 1994; Unruh *et al.*, 2003; Sawyer *et al.*, 2005; Wesnousky, 2005a). This same pattern is evident between the dextral Polaris fault and the normal Truckee fault zone (TFZ in Fig.1) 7 km to the southwest, which runs between Truckee across the head of

Independence Lake 16 km to the NNW (Olig *et al.*, 2005; S. Olig *et al.*, unpublished report, 2005, see Data and Resources) and continues another 16 km NNW into the southernmost corner of the Sierra Valley (Grose, 2000).

Truckee, California lies near the southwest corner of a broad shatter zone of high-angle conjugate strike-slip faults that is roughly bounded by the Little Truckee River on the north, the main stem of the Truckee River on the south, the TFZ on the west, and the Verdi Range on the east (Fig. 1). This area is central to a broader zone referred to as the Truckee transition zone (Schweickert *et al.*, 2004) that is defined by historic northwest- and northeast-oriented seismic trends (van Wormer and Ryall, 1980; Hawkins *et al.*, 1986; Ichinose *et al.*, 1999; Schweickert *et al.*, 2004; Smith *et al.*, 2008) that generally lack surface expression. At the core of this zone are the through-going Polaris fault and the conjugate DVFZ (Figs. 1a and 2b). Near Hobart Mills (Fig. 10), the dextral Polaris fault intersects north-striking east down normal faults of the ETFZ and the northeast-trending sinistral DVFZ (Fig. 10), demonstrating the complex nature of the spatially overlapping and kinematically linked faults that collectively accommodate the dextral transtension in this westernmost and structurally complex part of the NWL.

The Polaris and DVFZ are favorably oriented to accommodate the current regional stress field wherein the maximum principal stress (S_1 or P axis) is oriented horizontally in a north–south vertical plane and the minimum principal stress (S_3 or T axis) is oriented east–west, perpendicular to the north–south vertical plane (Wright, 1976; Zoback, 1989; Ichinose *et al.*, 2003; Schweickert *et al.*, 2004). At the Gray's Crossing site (Fig. 9), the intersection of high-angle conjugate faults defines fault-bounded quadrants that highlight the current regional stress field with contraction (previously described thrust faults) in the opposing north–south quadrants (P axis) and extension in the east–west quadrants (T axis). Furthermore, the orientation of the intersecting high-angle conjugate faults at the Gray's Crossing site (Fig. 9) matches the nodal plane orientation of moderate magnitude historical seismicity in the immediate area and the broader Truckee transition zone (Fig. 1; also Greensfelder, 1968; Tsai and Aki, 1970; van Wormer and Ryall, 1980; Hawkins *et al.*, 1986; and Schweickert *et al.*, 2004).

The largest historical earthquake in the vicinity of the Polaris fault happened on 12 September 1966 (Kachadoorian *et al.*, 1967). The M_L 6.0 Truckee earthquake occurred ~10 km northeast of Truckee on a nearly vertical northeast-striking fault with left-lateral displacement, as defined by the aftershock sequence (Greensfelder, 1968; Tsai and Aki, 1970). Surface manifestations of the earthquake included pressure ridges, mole tracks, and lurch cracks in alluvium

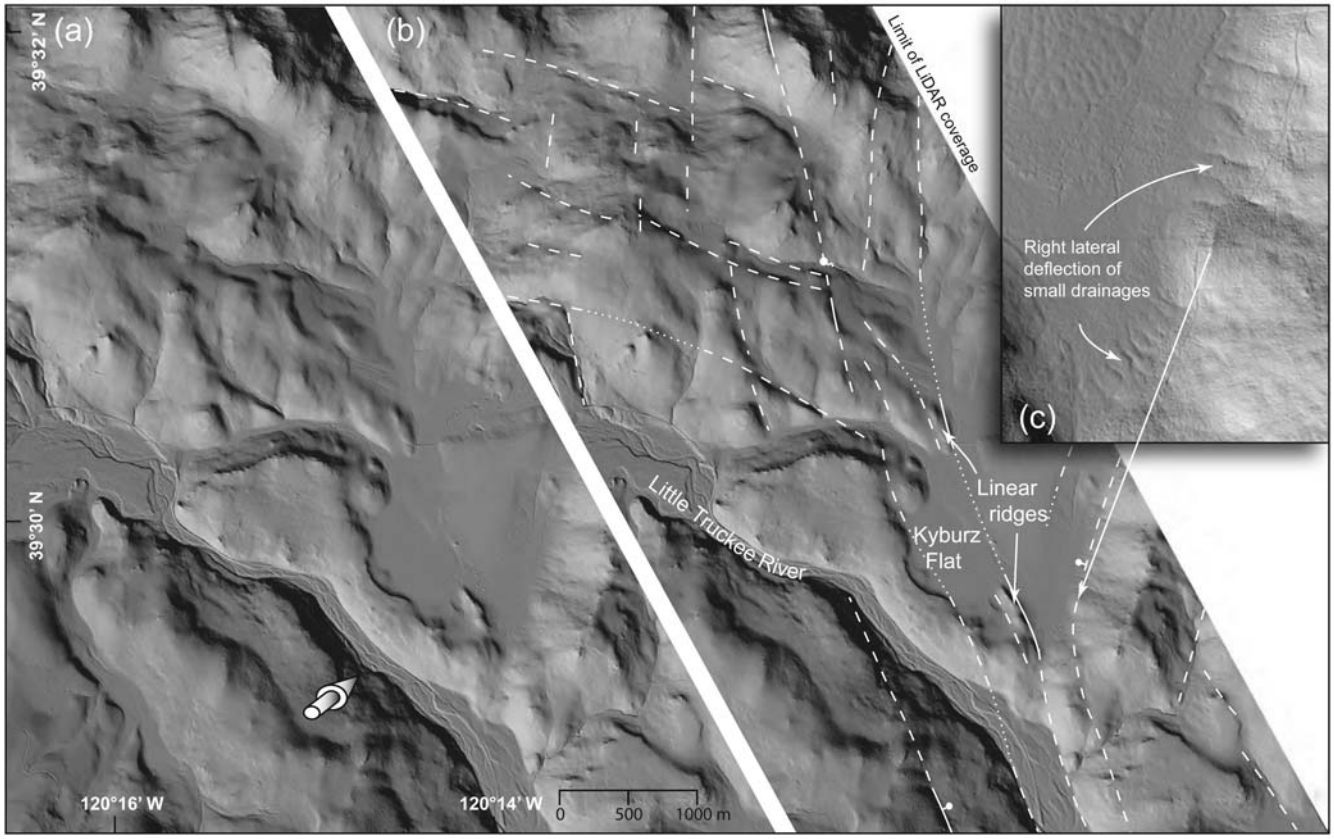

Figure 13. (a) Plan-view bare-earth LiDAR image of the area near Kyburz Flat. Shaded-gray arrow indicates direction of illumination (vertical exaggeration 2.5). (b) Solid white lines are mapped fault traces (dashed where approximately located, dotted where inferred, ball and bar on down-dropped side). (c) Enlargement showing right-lateral deflections of drainages along fault trace shown in (b).

along a ~16-km-long northeast-trending zone (Greensfelder, 1968), and Hawkins *et al.* (1986) associated the event with the DVFZ (Fig. 1a). Fault-plane mechanisms for the immediate area consistently show right-lateral motion on northwest-trending vertical planes and/or left-lateral motion on northeast-trending vertical planes (Tsai and Aki, 1970; van Wormer and Ryall, 1980; Hawkins *et al.*, 1986; Schweickert *et al.*, 2004).

Length of the Polaris Fault and Seismic Implications

As currently mapped using the airborne LiDAR imagery (Fig. 1), the previously unrecognized section of the Polaris fault extends for ~19 km from southeast of the Martis Valley, northwest across the Martis Creek reservoir and the Truckee basin, to Hobart Meadow north of Truckee. Geomorphic and geologic evidence suggests that the Polaris fault may extend an additional 17 km northwest. If so, the Polaris fault would be at least 36 km in length from a point 2 km south of the East Martis Creek fan to a point 6 km north of Kyburz Flat.

The ~35-km fault length makes the Polaris fault potentially capable of producing damaging large-magnitude earthquakes that could significantly threaten the Martis Creek Dam, which lies adjacent to the fault. Assuming a range of surface-rupture lengths (25, 30, and 35 km) and a range of depths to the base of the seismogenic zone (10, 14, and 18 km; Hawkins *et al.*, 1986 and Smith *et al.*, 2004), we estimate a range of earthquake magnitudes for the Polaris fault using the empirical relationships of Wells and Coppersmith (1994) and Hanks and Bakun (2002); these are listed in Table 2. These equations (Table 2) yield a range of possible maximum earthquake magnitudes (moment magnitude, M) for the Polaris fault from 6.4 to 6.9.

In addition, the southeasternmost mapped lineaments of the Mohawk Valley fault zone (Fig. 1) are only 5 km northwest of Kyburz Flat and may possibly connect or rupture coseismically with the Polaris fault, potentially making the previously mentioned estimates lower than credible maximums.

Geodetic versus Geologic Constraints of Deformation in the Northern Walker Lane

Numerous authors have noted the large differences between geodetically and geologically determined strain rates (by a factor of 2–3 times or greater) in the NWL (Thatcher and Wesnousky, 2001; Briggs and Wesnousky, 2001; Hammond and Thatcher, 2004; S. Olig *et al.*, unpublished report, 2005, see Data and Resources; Hammond and Thatcher, 2007). Geodetically constrained dextral motion for the westernmost part of the NWL (i.e., the MVFZ and Polaris fault trend) ranges from 2.3 ± 0.3 mm/yr (Hammond and Thatcher, 2007) to $\sim 6 \pm 3$ mm/yr (Dixon *et al.*, 2000). Geologically determined dextral slip rates for this westernmost part of the NWL are given by Sawyer *et al.* (2005), who reports a Holocene slip rate 0.3–0.5 mm/yr along an eastern strand of the MVFZ in the southern Sierra Valley (Fig. 1) and Howle *et al.* (2009), who reports a latest Pleistocene–Holocene slip rate of 0.4 ± 0.1 mm/yr for the Polaris fault east of Truckee. Geologic estimates of right-lateral slip across this westernmost part of the NWL are sparse which may largely explain the disparity between the geodetic and geologic strain rates.

Thatcher and Wesnousky (2001) conclude that discrepancies between geodetic and geologic rates in the Great Basin are due to a large fraction of the strain being distributed off of the main range-front bounding faults on smaller broadly distributed structures and unrecognized faults such as the Polaris fault. This assessment may well be the case for this westernmost part of the NWL where a significant fault has gone undetected, as well as adjacent subparallel structures.

From the north side of Truckee River ~1 and 3 km northeast of the Polaris site are at least two northwest-trending subparallel fault strands that cut flat-lying Donner Lake–age

Table 2
Calculated Maximum Earthquake Magnitudes for the Polaris Fault, Assuming a Range of Rupture Lengths and Depths*

Rupture Length (km)	Rupture Depth (km)	Rupture Area (km^2)	$M^\dagger$ Equation 1‡	$M^\dagger$ Equation 2§	$M^\dagger$ Equation 3$^\parallel$
25	10	250	6.7	6.4	6.4
25	14	350	6.7	6.6	6.5
25	18	450	6.7	6.7	6.6
30	10	300	6.8	6.5	6.5
30	14	420	6.8	6.6	6.6
30	18	540	6.8	6.7	6.7$^\#$
35	10	350	6.9	6.6	6.5
35	14	490	6.9	6.7	6.7
35	18	630	6.9	6.8	6.8$^\#$

*See text for discussion.
†Values of M are moment magnitudes.
$^\ddagger M = 5.08 + 1.16[\log(\text{surface-rupture length})]$; figure 9 in Wells and Coppersmith, 1994.
$^\S M = 4.07 + 0.98[\log(\text{rupture area})]$; figure 16 in Wells and Coppersmith, 1994.
$^\parallel M = \log(\text{rupture area}) + 3.98$; Hanks and Bakun, 2002.
$^\#$Where rupture area is greater than 537 km^2, $M = \frac{4}{3}[\log(\text{rupture area}) + 3.07]$; Hanks and Bakun, 2002.

outwash before crossing Prosser Creek Reservoir and forming prominent arms (linear drainages) on the north side of the reservoir (Figs. 1 and 8). Further north, these structures are expressed as aligned drainages that cut across the topographic divides between Prosser Creek, Sagehen Creek, and the Little Truckee River (Figs. 1 and 11). The NNW-trending scarps become more pronounced along strike to the north, where they bound the eastern margin of the Little Truckee River along the NNW-trending fault-controlled reach (Fig. 11). Similarly, west of the Polaris fault from Truckee to Independence Lake are numerous subparallel structures. Some of these have been mapped by Olig *et al.* (2005) and S. Olig *et al.* (unpublished report, 2005, see Data and Resources) as the ETFZ along the Highway 89 corridor, as well as the faults of the Truckee fault zone (TFZ in Fig. 1). However, west of Prosser Hill and east of the TFZ, the airborne LiDAR imagery reveals strong north-to-NNW-trending lineaments traversing the steep and densely vegetated terrain (Fig. 1). These structures do not display significant normal components, suggesting dextral motion is accommodated through this zone west of Highway 89 and east of the TFZ (Fig. 1). Dextral motion is also suggested in this area by the southeast-trending course of Prosser Creek through Carpenter Valley (west of the northeast-trending reach, DVFZ, in Fig. 1b), which is remarkably similar in appearance to the right-laterally offset reaches of Sagehen Creek and the Little Truckee River. The prominent NNW-trending fault that shutters Prosser Creek at Carpenter Valley (Fig. 1) also right-laterally offsets Tahoe-age lateral moraines at Independence Lake 10 km along strike to the NNW (Fig. 11a; Olig *et al.*, 2005). Between the west end of Independence Lake and Sagehen summit (~7 km to the east) are at least eight subparallel structures (Figs. 1 and 11). While most of these structures do not display the through-going nature of the Polaris fault to the east, their orientation is unmistakably related to the Polaris trend, and they are likely accommodating regional dextral transtention across this zone. The airborne LiDAR data could help direct future geologic investigations that in time might close the gap between geodetic and geologic strain rates. This in turn highlights the utility of bare-earth airborne LiDAR data in identifying and constraining tectonic geomorphology in densely vegetated terrain (e.g., Haugerud et al, 2003; Carter *et al.*, 2007; Prentice *et al.*, 2009).

Conclusions

The utilization of high-resolution bare-earth airborne LiDAR imagery greatly assisted in identifying, constraining, and visualizing the fault-related geomorphology in densely vegetated and otherwise inaccessible terrain. The likely active Polaris fault exhibits youthful and laterally continuous tectonic geomorphic features along the 35-km length currently mapped utilizing the LiDAR imagery.

Based on maximum limiting age constraints and statistically robust 3D modeling of an offset terrace riser, a preliminary minimum estimate of the latest Pleistocene–Holocene slip rate is 0.4 ± 0.1 mm/yr at the Polaris site east of Truckee.

Considering the favorable regional orientation as well as the strong and pervasive geomorphic character, the Polaris fault may be a prominent regional structure in accommodating dextral transtension in this westernmost part of the northern Walker Lane between Lake Tahoe and the Sierra Valley.

Conjugate fault patterns between the Polaris and Dog Valley fault zones are in strong coherence with moderate-magnitude historical seismicity of the immediate area, as well as the current regional stress regime.

Given the 35-km length, the Polaris fault is potentially a significant seismic hazard to the region and in particular to the Martis Creek Dam, with the capability of generating a magnitude 6.4–6.9 earthquake.

Data and Resources

The initial LiDAR data were collected by Merrick & Company for the Truckee Donner Public Utility District (TDPUD). The U.S. Army Corps of Engineers (USACE) gained access to these data under contract with TDPUD with a stipulation that USACE would not release the data to the public. These data remain proprietary to TDPUD.

The LiDAR data collected by Towell Surveying Mapping and GIS Services were acquired under contract with the USACE. These data are being used by USACE and its contractors to map and characterize faults in the region. These data will be released to the public at the conclusion of these studies, but the repository has not been determined as yet.

Ground-based LiDAR data reported in this paper were collected by J. F. Howle and are proprietary pending publication in a follow-up paper.

Faults referenced in the text are defined in the USGS Quaternary Fault and Fold Database, available at http://earthquake.usgs.gov/hazards/qfaults/ and from updated fault maps presented in a report by I. Wong, T. Dawson, P. Thomas, S. Olig, M. Dober, and F. Terra. This unpublished report, "Seismic Hazard Analyses and Development of Design Ground Motions for Martis Creek Dam, California," was prepared by URS Corp. Seismic Hazards Group on 6 March 2008 for the U.S. Army Corps of Engineers, Sacramento District. It is available upon request to the first author of this paper, L. E. Hunter.

The unpublished report by S. Olig, T. L. Sawyer, D. Wright, and F. Terra, "Preliminary Seismic Source Characterization of Faults near Stampede and Prosser Creek Dams–Washoe Project and Boca Dam–Truckee Storage Project," was prepared by URS Corp. Seismic Hazards Group on 28 June 2005 for the U.S. Bureau of Reclamation. It is available upon request to L. E. Hunter.

The classified point-cloud data were imaged using Quick Terrain (QT) Modeler by Applied Imagery (http://www.appliedimagery.com/qtmmain.htm). Vegetation was removed from the point-cloud data using TerraScan software by TerraSolid (http://www.terrasolid.fi/en/products/terrascan).

Other data used in this paper came from published sources listed in the references.

Acknowledgments

This work has been conducted under the U.S. Army Corps of Engineers' Dam Safety Assurance Program (DSAP). We thank DSAP program manager Richard Britzman and Martis Creek project manager Veronica Petrovsky for their continued support of our investigations, as well as the dam site manager, Dale Verner, who has provided logistical support through all phases of the project. The authors wish to thank Keith Kelson, Michael Rymer, Carol Prentice, and two anonymous reviewers for their constructive reviews of earlier drafts of this paper. The use of firm and/or brand names in this report is for identification purposes only and does not constitute endorsement by the United States government.

References

Bennett, R. A., N. A. Wernicke, A. Niemi, A. M. Friedrich, and J. L. Davis (2003). Contemporary strain rates in the northern Basin and Range province from GPS data, *Tectonics* **22,** no. 2, 1008, doi 10.1029/2001TC001355.

Benson, L. V., D. R. Currey, R. I. Dorn, K. R. Lajoie, C. G. Oviatt, S. W. Robinson, G. I. Smith, and S. Stine (1990). Chronology of expansion and contraction of four Great Basin lake systems during the past 35,000 years, *Palaeogeography, Palaeoclimatology, Palaeoecology* **78,** 241–286.

Birkeland, P. W. (1963). Pleistocene volcanism and deformation of the Truckee area, north of Lake Tahoe, California, *GSA Bull.* **74,** 1453–1464.

Birkeland, P. W. (1964). Pleistocene glaciation of the northern Sierra Nevada, north of Lake Tahoe, California, *J. Geol.* **72,** 810–825.

Briggs, R. W., and S. G. Wesnousky (2001). The Basin and Range-Sierra Nevada transition along the northern Walker Lane: Geology vs. geodesy, *Seismol. Res. Lett.* **72,** no. 2, 280.

Bursik, M. I., and A. R. Gillespie (1993). Late Pleistocene glaciation of Mono Basin, California, *Quat. Res.* **39,** 24–35.

Carter, W. E., R. L. Shrestha, and K. C. Slatton (2007). Geodetic laser scanning, *Phys. Today* **60,** 41–47.

Clark, D. H., and A. R. Gillespie (1997). Timing and significance of late-glacial and Holocene cirque glaciation in the Sierra Nevada, California, *Quat. Int.* **38/39,** 21–28.

Cowgill, E. (2007). Impact of riser reconstructions on estimation of secular variation in rates of strike-slip faulting: Revisiting the Cherchen River site along the Altyn Tagh Fault, NW China, *Earth Planet. Sci. Lett.* **254,** 239–255.

Crampton, T., R. Rubin, C. Slack, and W. McCormick (2009). Preliminary results of paleoseismic trenching and geomorphic mapping of the Polaris fault, Truckee, CA, 2009 Association of Environmental and Engineering Geologists Annual Meeting, Program with Abstracts, *AEG News* **52,** 65.

Dixon, T. H., M. Miller, F. Farina, H. Wang, and D. Johnson (2000). Present-day motion of the Sierra Nevada block and some tectonic implications for the Basin and Range Province, North American Cordillera, *Tectonics* **19,** 474–486.

Dixon, T. H., S. Robaudo, J. Lee, and M. C. Reheis (1995). Constraints on present-day Basin and Range deformation from space geodesy, *Tectonics* **14,** 755–772.

Faulds, J. E., and C. D. Henry (2008). Tectonic influences on the spatial and temporal evolution of the Walker Lane: An incipient transform fault along the evolving Pacific—North American plate boundary, *Arizona Geol. Soc. Digest* **22,** 437–470.

Faulds, J. E., C. D. Henry, and N. H. Hinz (2005). Kinematics of the northern Walker Lane: An incipient transform fault along the Pacific-North American plate boundary, *Geology* **33,** 505–508.

Gillespie, A. R. (1991). Testing a new climatic interpretation for the Tahoe glaciation.*White Mountain Research Station Symposium* 3**,** 383–398.

Gold, R. D., E. Cowgill, J. R. Arrowsmith, J. Gosse, X. Chen, and X. F. Wang (2009). Riser diachroneity, lateral erosion, and uncertainty in rates of strike-slip faulting: A case study from Tuzidun along the Altyn Tagh fault, NW China, *J. Geophys. Res.* **114,** no. B04401, doi 10.1029/2008JB005913.

Greensfelder, R. (1968). Aftershocks of the Truckee, California, earthquake of September 12, 1966, *Seismol. Soc. Am. Bull.* **58,** no. 5, 1607–1620.

Grose, T. T. L. (2000). Geologic map of the Sierraville 15′ quadrangle, Sierra and Plumas counties, California, *CDMG Open-File Report 2000-24*.

Hallet, B., L. E. Hunter, and J. Bogen (1996). Rates of erosion and sediment evacuation by glaciers: A review of field data and their implications, *Global Planet. Change* **12,** 213–235.

Halpin, E. C., and K. A. Ferguson (2007). US Army Corps of Engineers dam safety program status and lessons learned in transitioning to risk informed approaches, *J. Dam Safety* **5,** no. 2, 24–36.

Hammond, W. C., and W. Thatcher (2004). Contemporary tectonic deformation of the Basin and Range province, western United States: 10 years of observation with the Global Positioning System, *J. Geophys. Res.* **109,** no. B08403, 21 pp., doi 10.1029/2003JB002746.

Hammond, W. C., and W. Thatcher (2007). Crustal deformation across the Sierra Nevada, northern Walker Lane, Basin and Range transition, western United States measured with GPS, 2000–2004, *J. Geophys. Res.* **112,** no. B05411, 26 pp., doi 10.1029/2006JB004625.

Hanks, T. C., and W. H. Bakun (2002). A bilinear source-scaling model for $\mathbf{M}$ − log A observations of continental earthquakes, *Bull. Seismol. Soc. Am.* **92,** 1841–1846.

Harkins, N., and E. Kirby (2008). Fluvial terrace riser degradation and determination of slip rates on strike-slip faults: An example from the Kunlan fault, China, *Geophys. Res. Lett.* **35,** L05406, doi 10.1029/2007GL033073.

Haugerud, R. A., D. J. Harding, S. Y. Johnson, J. L. Harles, and C. S. Weaver (2003). High-resolution LiDAR topography of the Puget Lowland, Washington—A bonanza for Earth science, *GSA Today* **13,** no. 6, 4–10.

Hawkins, F. F., R. LaForge, and R. A. Hansen (1986). Seismotectonic study of the Truckee/Lake Tahoe area northeastern Sierra Nevada, California, *U.S. Bureau of Reclamation Seismotectonic Report Number 85-4*, 210 p.

Howle, J. F., R. C. Finkel, and G. Seitz (2005). Cosmogenic exposure ages of Tioga and Tahoe age moraines at Meeks Bay, Lake Tahoe, California, *GSA Abstr. Programs* **37,** no. 7, 232.

Howle, J. F., G. W. Bawden, L. E. Hunter, and R. S. Rose (2009). Modeling right-lateral offset of a Late Pleistocene terrace riser along the Polaris fault using ground-based LiDAR imagery, abstract no. G51B-0661, *American Geophysical Union*, Fall Meeting, 14–18 December 2009, San Francisco, California.

Hunter, L. E., R. S. Rose, J. F. Howle, V. W. Brown, M. H. Powers, B. Hilton, and E. Hubbard (2009). *AEG 2009 Annual Meeting Field Trip Guidebook: Geotechnical and Paleoseismic Investigations of the Martis Creek Dam, Truckee, California*, Association of Environmental and Engineering Geologists, Denver, CO, 44 p.

Ichinose, G., J. Anderson, K. Smith, D. dePolo, R. Anooshehpoor, R. A. Schweickert, and M. M. Lahren (1999). The seismotectonics of the 30 October 1998 Incline Village, Nevada, earthquake and its effects, *Seismol. Res. Lett.* **70,** 297–305.

Ichinose, G. A., J. G. Anderson, K. D. Smith, and Z. Yuehua (2003). Source parameters of eastern California and western Nevada earthquakes from regional moment tensor inversion, *Bull. Seismol. Soc. Am.* **93,** no. 1 61–84.

Ichinose, G. A., K. D. Smith, and J. G. Anderson (1998). Moment tensor solutions of the 1994 to 1996 Double Spring Flat, Nevada, earthquake sequence and implications for local tectonic models, *Bull. Seismol. Soc. Am.* **88,** no. 6, 1363–1378.

James, L. A., J. Harbor, D. Fabel, D. Dahms, and D. Elmore (2002). Late Pleistocene glaciations in the northwestern Sierra Nevada, California, *Quat. Res.* **57,** 409–419.

Kachadoorian, R., R. F. Yerkes, and O. A. Waananen (1967). Effects of the Truckee, California, earthquake of September 12, 1966, *USGS Circular* **537,** 14.

Latham, T. S. (1985). Stratigraphy, structure, and geochemistry of Plio-Peistocene volcanic rocks of the western Basin and Range province, near Truckee, California, *Ph.D. dissertation*, Univsity of California at Davis341 pp.

Melody, A. (2009). Holocene faulting and Late Quaternary paleohydrology in the northwestern Walker Lane north of Truckee, California, 2009 Association of Environmental and Engineering Geologists Annual Meeting, Program with Abstracts, *AEG News* **52,** 91.

Olig, S., T. L. Sawyer, L. Anderson, D. Wright, I. Wong, and F. Terra (2005). Insights into Quaternary strain patterns in the northern Walker Lane from mapping and source characterization of faults near Truckee, California, *Seismol. Res. Lett.* **76,** no. 2, 251.

Oskin, M. E., K. Le, and M. D. Strane (2007). Quantifying fault-zone activity in arid environments with high-resolution topography, *Geophys. Res. Lett.* **34,** L23S05, doi 10.1029/2007GL031295.

Page, W. D., T. L. Sawyer, M. K. McLaren, W. U. Savage, and J. Wakabayashi (1993). The Quaternary Tahoe-Medicine Lake trough: The western margin of the Basin and Range transition, NE California, *GSA Abstr. Programs* **25,** 131.

Prentice, C. S., C. J. Crosby, C. S. Whitehill, J. R. Arrowsmith, and K. P. Furlong (2009). Illuminating Northern California's active faults, *Eos* **90,** 7, 55–56.

Repka, J. L., R. S. Anderson, and R. C. Finkel (**1997**). Cosmogenic dating of fluvial terraces, Fremont River, Utah, *Earth Planet. Sci. Lett.* **152,** 59–73.

Sawyer, T. L., and R. W. Briggs (2001). Stop 9: Kinematics and late Quaternary activity of the Mohawk Valley fault zone, *Pacific Cell Friends of the Pleistocene 2001 Fall Field Trip Guidebook*, Friends of the Pleistocene, Pacific Cell, San Francisco, California, 49–62.

Sawyer, T. L., R. W. Briggs, and A. R. Ramelli (2005). Late Quaternary activity of the southern Mohawk Valley fault zone, Northeastern California, *Seismol. Res. Lett.* **76,** no. 2, 248–249.

Sawyer, T. L., W. D. Page, and M. A. Hemphill-Haley (1995). Southern Mohawk Valley fault zone at the Calpine trench site, in W. D. Page (Editor), *Quaternary Geology along the Boundary between Modoc Plateau, Southern Cascade Mountains, and Northern Sierra Nevada: Friends of the Pleistocene 1995 Pacific Cell Field Trip Guidebook*, Friends of the Pleistocene, Pacific Cell, San Francisco, California.

Schweickert, R. A., M. M. Lahren, R. E. Karlin, K. D. Smith, J. F. Howle, and G. Ichinose (2004). Transtensional deformation in the Lake Tahoe region, California and Nevada, USA, *Tectonophysics* **392,** 303–323.

Shackleton, N. J., and N. D. Opdyke (1976). Oxygen-isotope and paleomagnetic stratigraphy of Pacific core V28-239 late Pliocene to latest Pleistocene, R. M. Cline and J. D. Hays (Editors), *Geol. Soc. Am. Memoir*, Vol. **145**, 449–464.

Smith, K., D. von Seggern, D. dePolo, J. Anderson, G. Biasi, and R. Anooshehpoor (2008). Seismicity of the 2008 Mogul—Somersett west Reno, Nevada, earthquake sequence, Fall Meet. Suppl.*Eos Trans. Am. Geophys. Union* **89,** no. 53, abstract S53C-02.

Smith, K. D., D. von Seggern, G. Blewitt, L. Preston, J. G. Anderson, B. P. Wernicke, and J. L. Davis (2004). Evidence for deep magma injection beneath Lake Tahoe, Nevada—California, *Science* **305,** 1277–280.

Stewart, J. H. (1988). Tectonics of the Walker Lane belt, western Great Basin: Mesozoic and Cenozoic deformation in a zone of shear, in W. G. Ernst (Editor), *The Geotectonic Development of California*, Prentice-Hall, Englewood Cliffs, New Jersey, 683–713.

Sylvester, A. G., W. S. Wise, J. T. Hastings, and L. A. Moyer (2007). New digital geologic map of the northern Lake Tahoe-Donner Pass region, Sierra Nevada, California, *GSA Abstr. Programs* **39,** no. 5.

Thatcher, W., and S. G. Wesnousky (2001). Character and origin of discrepancies between Holocene and GPS fault slip rate estimates in the interior western U.S., *Seismol. Res. Lett.* **72,** no. 2, 280.

Thatcher, W., G. R. Foulger, B. R. Julian, J. Svarc, E. Quilty, and G. W. Bawden (1999). Present day deformation across the Basin and Range province, western United States, *Science* **283,** 1714–1718.

Tsai, Y. B., and K. Aki (1970). Source mechanism of the Truckee, California earthquake of September 12, 1966, *Seismol. Soc. Am. Bull.* **60,** no. 4, 1199–1208.

Unruh, J., J. Humphrey, and A. Barron (2003). Transtensional model for the Sierra Nevada frontal fault system, eastern California, *Geology* **31,** no. 4, 327–330.

U.S. Army Corps of Engineers (1966). *Martis Creek Reservoir, Truckee River, Basin, Nevada and California: Site Geology*, Design Memorandum No. 8, U.S. Army Corps of Engineers, Sacramento, California, 19 pp.

U.S. Army Corps of Engineers (1972). *Martis Creek Lake Dam and Appurtenances, Truckee River Basin, Nevada and California: Foundation Report*, U.S. Army Corps of Engineers, Sacramento, California, 107 pp.

van Wormer, J. D., and A. D. Ryall (1980). Sierra Nevada—Great Basin boundary zone: Earthquake hazard related to structures, active tectonic processes, and anomalous patterns of earthquake occurrence, *Seismol. Soc. Am. Bull.* **70,** 1557–1572.

Wells, D., and K. J. Coppersmith (1994). New empirical relationships among magnitude, rupture length, rupture width, rupture area and surface displacement, *Bull. Seismol. Soc. Am.* **84,** 974–1002.

Wesnousky, S. G. (2005a). The San Andreas and Walker Lane fault systems, western North America: Transpression, transtension, cumulative slip and the structural evolution of a major transform plate boundary, *J. Struct. Geol.* **27,** 505–1512.

Wesnousky, S. G. (2005b). Active faulting in the Walker Lane, *Tectonics* **24,** TC3009, 35 pp., doi 10.1029/2004TC001645.

Wesnousky, S. G., and C. H. Jones (1994). Oblique slip, slip partitioning, spatial and temporal changes in the regional stress field, and relative strength of active faults in the Basin and Range, western United States, *Geology* **22,** 1031–1034.

Wright, L. (1976). Late Cenozoic fault patterns and stress fields in the Great Basin and westward displacement of the Sierra Nevada block, *Geology* **4,** 489–494.

Yount, J. C., and D. D. La Pointe (1997). Glaciation, faulting, and volcanism in the southern Lake Tahoe basin, in: *Field Trip Guidebook for the National Association of Geoscience Teachers, Far West Section, 1997 Fall Conference*, Western Nevada Community College, Fallon, Nevada, II-1–II-22.

Zoback, M. L. (1989). State of stress and modern deformation of the northern Basin and Range Province, *J. Geophys. Res.* **94,** 7105–7128.

U.S. Army Corps of Engineers
Sacramento, California 95814
(L.E.H., R.S.R.)

U.S. Geological Survey
Carnelian Bay, California 96140
(J.F.H.)

U.S. Geological Survey
Sacramento, California 95819
(G.W.B.)

Manuscript received 2 September 2009